AD-A155 560 ELECTRICAL AND MECHANICAL PROPERTIES OF INTERCALATED GRAPHITE FIBERS(U) CELANESE RESEARCH CO SUMMIT NJ H A GOLDBERG APR 85 ARO-17260.7-PH DAAG29-81-C-0016 1/1

UNCLASSIFIED F/G 11/5 NL

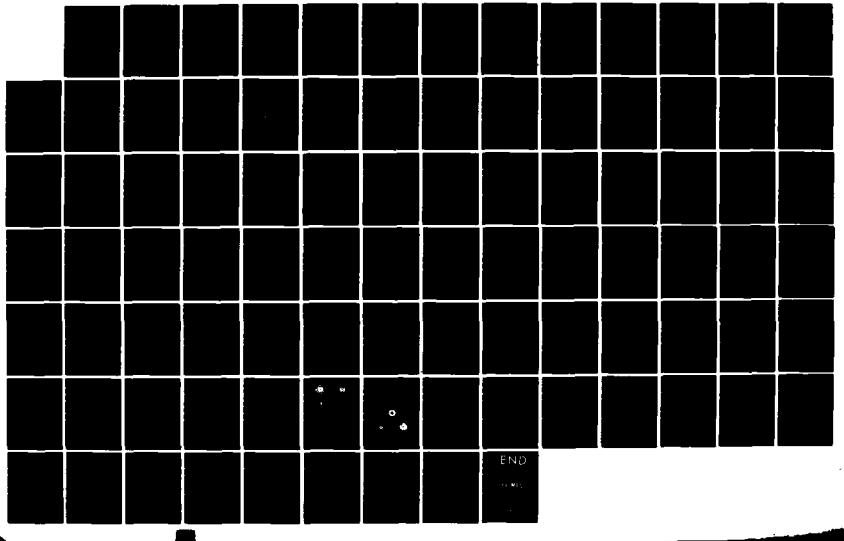

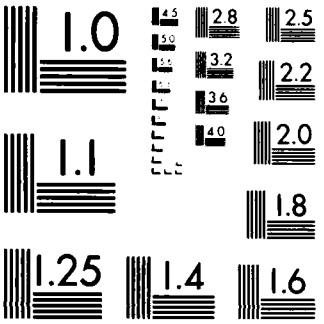

ELECTRICAL AND MECHANICAL PROPERTIES OF INTERCALATED GRAPHITE FIBERS

FINAL REPORT

Harris A. Goldberg

April 1985

U. S. ARMY RESEARCH OFFICE

CONTRACT DAAG29-81-C-0016

CELANESE RESEARCH COMPANY
86 Morris Avenue
Summit, New Jersey 07901

Approved for Public Release - Distribution Unlimited

THE VIEW, OPINIONS, AND/OR FINDINGS CONTAINED IN THIS REPORT ARE THOSE OF THE AUTHOR(S) AND SHOULD NOT BE CONSTRUED AS AN OFFICIAL DEPARTMENT OF THE ARMY POSITION, POLICY, OR DECISION, UNLESS SO DESIGNATED BY OTHER DOCUMENTATION.

UNCLASSIFIED

SECURITY CLASSIFICATION OF THIS PAGE *(When Data Entered)*

REPORT DOCUMENTATION PAGE		READ INSTRUCTIONS BEFORE COMPLETING FORM
1. REPORT NUMBER ARO 17260.7-PH	2. GOVT ACCESSION NO. AD-A155 560 N/A	3. RECIPIENT'S CATALOG NUMBER N/A
4. TITLE *(and Subtitle)* ELECTRICAL AND MECHANICAL PROPERTIES OF INTERCALATED GRAPHITE FIBERS		5. TYPE OF REPORT & PERIOD COVERED Final April 1981 - April 1984 6. PERFORMING ORG. REPORT NUMBER
7. AUTHOR(s) Harris A. Goldberg		8. CONTRACT OR GRANT NUMBER(s) DAAG29-81-C-0016
9. PERFORMING ORGANIZATION NAME AND ADDRESS Celanese Corporation Celanese Research Company 86 Morris Avenue, Summit, NJ 07901		10. PROGRAM ELEMENT, PROJECT, TASK AREA & WORK UNIT NUMBERS
11. CONTROLLING OFFICE NAME AND ADDRESS U. S. Army Research Office Post Office Box 12211 Research Triangle Park, NC 27709		12. REPORT DATE April 1985 13. NUMBER OF PAGES 87
14. MONITORING AGENCY NAME & ADDRESS*(if different from Controlling Office)*		15. SECURITY CLASS. *(of this report)* Unclassified 15a. DECLASSIFICATION/DOWNGRADING SCHEDULE

16. DISTRIBUTION STATEMENT *(of this Report)*

Approved for public release; distribution unlimited.

17. DISTRIBUTION STATEMENT *(of the abstract entered in Block 20, if different from Report)*

NA

18. SUPPLEMENTARY NOTES

The view, opinions, and/or findings contained in this report are those of the author(s) and should not be construed as an official Department of the Army position, policy, or decision, unless so designated by other documentation.

19. KEY WORDS *(Continue on reverse side if necessary and identify by block number)*

Carbon Fibers, Graphite Fibers, Electrical Properties, Intercalated Graphite, Electromechanical Properties, Piezoresistance, X-ray Diffraction, Resistance vs. Temperature, Intercalation, X-ray Absorption, XANES, AsF_5.

20. ABSTRACT *(Continue on reverse side if necessary and identify by block number)*

In order to understand the electrical and mechanical property changes which occur when graphite fibers are intercalated, it is essential that a better understanding of the properties of the fibers prior to intercalation be developed. Research aimed at elucidating the structure-property relationships in neat carbon and graphite fibers is presented. In particular, the changes with increasing heat treatment in both electronic and structural properties are discussed. The relative importance of crystallite

DD FORM 1 JAN 73 1473 EDITION OF 1 NOV 65 IS OBSOLETE

UNCLASSIFIED

SECURITY CLASSIFICATION OF THIS PAGE *(When Data Entered)*

size, three dimensional order, and the details of disordered regions between crystallites are demonstrated by analysis of: resistance versus temperature; piezoresistance; x-ray diffraction; and intercalation behavior. Crystallite size effects must be included in order to understand the electronic structure of the fibers studied here. Arguments which demonstrate the potential importance of the disordered regions between crystallites to the anamolous resistance-temperature behavior of low-modulus, high-strength fibers are presented.

Three dimensional order is shown to increase continously with heat treatment. Generally, one can only intercalate high-modulus fibers which clearly exhibit three dimensional order. However, when sufficiently strong electron acceptors are used, fibers which don't have any well-defined stacking order can be intercalated. The degree of three dimensional order is shown to be related to the negative piezoresistance observed in high-modulus fibers. The piezoresistance of carbon and graphite fibers is discussed in terms of a simple polycrystalline model, and useful qualitative information on the parameters needed for modelling the elastic properties of these materials is obtained.

FORWARD

This report will serve two purposes: to review the results of our research on carbon and graphite fibers which has already been published; and provide a preliminary report of some of our more recent work which has not yet been prepared for publication. In Section III (Summary of Results), all the important results are outlined. The details of the published results are included in the appendices. Sections IV-VI include short descriptions of additional work done under this contract which is not yet ready for publication. Thus, the material included here should be viewed as preliminary results.

This work was done with the help and collaboration of a large number of people. Let me begin by thanking Dr. I. L. Kalnin for his help and encouragement; particularly during the early phases of this project. Professor I. L. Spain was an invaluble collaborator in almost every area described in this report. I would also like to thank Dr. J. B. Stamatoff not only for his x-ray diffraction work, but also for his contributions toward the overall understanding of carbon and graphite fibers. Dr. S. Heald collaborated with us on the x-ray absorption experiments at CHESS. Drs. F. M. Marikar and D. Nikles did the metal-chloride intercalations. Special thanks go to G. Breckenridge for his technical assistance and especially for his patient help with the difficult preparations and handling of AsF_5 compounds. K. Volin helped with some of the resistance versus temperature experiments, as did L. McKenzie and B. Bauer. F Haimbach did the mechanical testing, with the assistance of G. Babcock. F. Warner provided technical assistance in the x-ray diffraction laboratory.

ABSTRACT

In order to understand the electrical and mechanical property changes which occur when graphite fibers are intercalated, it is essential that a better understanding of the properties of the fibers prior to intercalation be developed. Research aimed at elucidating the structure-property relationships in neat carbon and graphite fibers is presented. In particular, the changes with increasing heat treatment in both electronic and structural properties are discussed. The relative importance of crystallite size, three dimensional order, and the details of disordered regions between crystallites are demonstrated by analysis of: resistance versus temperature; piezoresistance; x-ray diffraction; and intercalation behavior. Crystallite size effects must be included in order to understand the electronic structure of the fibers studied here. Arguments which demonstrate the potential importance of the disordered regions between crystallites to the anamolous resistance-temperature behavior of low-modulus, high-strength fibers are presented.

Three dimensional order is shown to increase continuously with heat treatment. Generally, one can only intercalate high-modulus fibers which clearly exhibit three dimensional order. However, when sufficiently strong electron acceptors are used, fibers which don't have any well-defined stacking order can be intercalated. The degree of three dimensional order is shown to be related to the negative piezoresistance observed in high-modulus fibers. The piezoresistance of carbon and graphite fibers is discussed in terms of a simple polycrystalline model, and useful qualitative information on the parameters needed for modelling the elastic properties of these materials is obtained.

TABLE OF CONTENTS

I.	STATEMENT OF THE PROBLEM	1
II.	SUMMARY OF MOST IMPORTANT RESULTS	1
	1. ELECTRICAL PROPERTIES OF NEAT FIBERS	1
	2. THREE DIMENSIONAL ORDER	2
	3. PIEZORESISTANCE OF CARBON AND GRAPHITE FIBERS	3
	4. INTERCALATION OF ACCEPTORS INTO CARBON AND GRAPHITE FIBERS	4
III.	ELECTRICAL PROPERTIES OF CARBON AND GRAPHITE FIBERS	5
IV.	PIEZORESISTANCE OF CARBON AND GRAPHITE FIBERS	10
	1. PIEZORESISTANCE THEORY	11
	2. THEORY OF MECHANICAL PROPERTIES	13
	3. ORIENTATION	14
	4. THREE-DIMENSIONAL ORDER	21
	5. RESULTS FROM PIEZORESISTANCE	21
	6. HYDROSTATIC PRESSURE EXPERIMENTS	32
	7. OTHER EFFECTS	35
	8. SUMMARY AND CONCLUSIONS	37
V.	PROPERTIES OF INTERCALATED FIBERS	38
VI.	CONCLUSIONS AND SUGGESTED FUTURE WORK	43
REFERENCES		45
PUBLICATIONS		47
APPENDIX I.	ELECTRONIC PROPERTIES OF PAN-BASED CARBON FIBERS - I	48
APPENDIX II.	AN UNUSUAL RESISTIVITY MAXIMUM IN LOW MODULUS CARBON FIBERS	59
APPENDIX III.	X-RAY DIFFRACTION STUDIES OF STRUCTURAL DIMENSIONALITY IN CARBON FIBERS	61
APPENDIX IV.	X-RAY ABSORPTION STUDIES OF LOW CONCENTRATION AsF_5 INTERCALATION COMPOUNDS	67

LIST OF FIGURES

Page No.

Figure 1. Magnitude of Negative Temperature Coefficient of Resistance in Carbon and Graphite Fibers Plotted Versus Heat Treatment Temperature on A Log Scale 7

Figure 2. A Calculation of Young's Modulus Versus Crystallite Orientation is Shown for Various Choices of S_{44} 16

Figure 3. Poisson Ratio Versus Orientation 17

Figure 4. The Ratio of C-Axis Strain to Elongation Versus Orientation 17

Figure 5. 002 Rocking Curves for Ex-PAN and Ex-Pitch Fibers 18

Figure 6. 11ℓ Diffraction Scans for Ex-PAN and Ex-Pitch Fibers 22

Figure 7. Piezoresistance of Ex-PAN Fibers 26

Figure 8. Piezoresistance of Ex-Pitch Fibers 27

Figure 9. Piezoresistance Versus Young's Modulus 29

Figure 10. Piezoresistance of $CuCl_2$ Intercalated Fiber 33

LIST OF TABLES

		Page No.
Table 1.	Parameters Obtained from Simple Two-Band Model	9
Table 2.	Lifetime Broadening	9
Table 3.	Elastic Constants of Graphite Crystals	15
Table 4.	Misorientation Distribution	20
Table 5.	S_{44} from Young's Modulus	20
Table 6.	Hydrostatic Pressure	35

I. STATEMENT OF THE PROBLEM

The original goal of this work was to elucidate the interrelationships of the microstructure of graphite fibers, the intercalation process, and the electrical and mechanical property changes resulting from intercalation. In order to pursue this goal effectively, it was also necessary to improve our understanding of the structure-property relationships in neat carbon and graphite fibers. We therefore addressed the following specific subjects:

1. the changes in electronic properties with increasing heat treatment and its relationship to structural development;

2. quantification of the degree of three dimensional order which occurs upon heat treatment and its role in determining electrical and chemical properties;

3. piezoresistance of carbon and graphite fibers; and,

4. intercalation of electron acceptors (such as AsF_5) into fibers.

Other work included some preliminary intercalations of metal-chlorides into both ex-pitch and ex-PAN fibers. This is an area which has been receiving increasing attention in the literature over the past few years.[1-3]

II. SUMMARY OF MOST IMPORTANT RESULTS

1. Electrical Properties of Neat Fibers

Our first important result was to recognize that the increasing temperature dependence of the resistance of graphite fibers with increasing heat treatment could be quantitatively un-

derstood using simple band models previously used for other pyrocarbons. (See the publication included here as Appendix I.) The band overlap, however had to be decreasing with increasing heat treatment, and this was contrary to what is expected of a homogeneous carbon where the crystallite size and three dimensionality increases with increasing heat treatment. As discussed later in this report, we have recently shown that if one includes lifetime broadening of the electronic states (through the uncertainty principle, for example) that the band overlap required to explain the resistance versus temperature behavior can be understood.

The above discussion applies only to what is usually referred to as graphite fibers. The more commonly used high strength carbon fibers are more disordered and have a significantly smaller crystallite size. Our estimates of the lifetimes of the delocalized band states within a crystallite indicate that these materials may have their conductivity dominated by electron transfer across crystal boundaries and/or through disordered regions of the fiber. Experimentally, we have found that these fibers have an unusual maximum in their resistance at about 30°K. Thus, one might expect to find electrical characteristics which are qualitatively different in high strength carbon fibers from those of graphite fibers. The resistance of high strength carbon fibers decreases with decreasing temperature below 30°K all the way to 1°K. A publication showing data down to 1.8°K is included in Appendix II.

2. Three Dimensional Order

Before the Celanese work, it was generally believed that fibers made from polyacrylonitrile (ex-PAN) were always turbostratic, i.e. they did not have any order to the stacking sequence of the hexagonal basal planes. Work done just prior to this contract demonstrated that, when ex-PAN fibers were prepared with a

modulus of near 690 GPa (100Msi), that there was evidence for three dimensional order. More recently, we have demonstrated that even commercially available GY-70 ex-PAN fibers have three dimensional stacking order. This is discussed in detail in Appendix III.

The existence of three dimensional stacking order is important if one is attempting to model the properties of graphite fibers. Bright[4] has already shown the importance of the three dimensionalty of fibers to understanding their low temperature magnetoresistance. We will discuss the importance of the three dimensional order to our understanding of electro-mechanical properties of fibers in the next section. In addition, since only high modulus fibers can usually be intercalated, one might suspect that three dimensional order has something to do with the ease with which intercalation can take place. Although, the importance of three dimensional order can not be fully assessed at the present time, we have been able to intercalate a 345 GPa (50Msi) pitch fiber to stage 2 with AsF_5. This fiber does not show any clear evidence for long ranged stacking order.

Finally, we have demonstrated that the growth of three dimensional order is continuous as fibers are heat-treated. We do not see any evidence in x-ray diffraction for the existence of two phases: one turbostratic and one three dimensional.

3. Piezoresistance of Carbon and Graphite Fibers

Negative piezoresistance has been known in carbon and graphite fibers and was first reported by Owsten[5]. Although several mechanisms have been suggested, there had been few serious attempts to model the electromechanical properties of fibers. (The most detailed investigation done to date was by Komaki.[6]) We have recently shown that negative piezoresistance in both ex-PAN and ex-pitch fibers can be understood in terms of electron carrier

density changes which occur only in three dimensionally ordered fibers. This work also has important implications for the development of better polycrystalline elastic models for these materials, and will be discussed in more detail in Section V.

Negative piezoresistance was also observed in P-100 (an ex-pitch fiber with modulus near 690 GPa) intercalated with $FeCl_3$. This may imply that the charge transfer to the graphite planes is strain (and pressure) dependent in this material.

4. Intercalation of Acceptors into Carbon and Graphite Fibers

We have shown that when strong acceptors are intercalated into both ex-pitch and ex-PAN fibers, many well defined stages can readily be observed.[7] This is contrary to what has been reported when weaker acceptors such as $FeCl_3$ are used.[8] (Stages have been observed in boron-loaded ex-PAN fibers intercalated with metal chlorides,[9] but significant amounts of graphite remain unreacted.) The highest stage we have observed is stage 9 (which has a repeat distance of 35Å)in a low concentration (18.5% by weight) AsF_5-intercalated ex-PAN fiber. The observation of such a long period superstructure in a material as disordered as a graphite fiber is remarkable. Furthermore, if we assume an in-plane packing of 8 carbons per AsF_5 unit, the expected concentration of a stage 9 compound is 19.7%. The excellent agreement between this calculated concentration and the measured weight uptake implies that the fibers have intercalated to stage 9 homogeneously.

In order to elucidate the mechanism of acceptor intercalation, and demonstrate any differences between intercalation in fibers as compared with more ordered graphites, a number of studies of low concentration AsF_5-graphite fiber compounds were made. Samples with a weight uptake of less than 17% did not show

any change in x-ray diffraction, although the reaction of the AsF_5 was clearly observed via x-ray absorption. Near-edge x-ray absorption measurements (done at CHESS in collaboration with S. Heald of Brookhaven) indicated that these samples underwent extensive charge transfer between the graphite and the AsF5. If the As^{+3} species is assumed to be AsF_3,[10] then one finds that the charge transfer reaction:

$$2e^- + 3AsF_5 \longrightarrow 2AsF_6^- + AsF_3$$

goes to completion. However, the AsF_3 is found to be oriented in the fibers, and the orientation is so large as to indicate that the AsF_3 bonds must be distorted. In addition, cryopumping can reversably remove the oriented As^{+3} species. These results may imply that there is another species other than AsF_3, AsF_5, and AsF_6 in low concentration fiber samples. More details of this work are found in Appendix IV and Section VI.

III. ELECTRICAL PROPERTIES OF CARBON AND GRAPHITE FIBERS

In this section, I will briefly review the results presented in the publication included as Appendix I, and then proceed to describe the importance of estimating the carrier lifetime and the associated energy leveling broadening in carbon and graphite fibers.

The primary purpose of this work is to explore the extent to which the properties of carbon and graphite fibers can be understood in terms of the known and/or expected properties of graphite crystallites and aromatic carbon planes. Graphite is an hexagonal crystal in which the basal planes are in an ABAB stacking. Since the interplane spacing is large (3.35Å), the electrical and mechanical properties are anisotropic. The band structure of graphite consists of electron and hole bands which meet at the

edge of the Brillouin zone, and in fact overlap a small (0.025ev) amount because of the weak interplanar interaction. Graphite is thus a semimetal in which the carrier density is temperature dependent but remains finite at zero degrees Kelvin, even in a perfect crystal. The in-plane electron (and hole) mobilites are exceptionally high due to the tightly bound aromatic structure. This high mobility persists even when the carrier concentration is increased by intercalation with electron acceptors such as AsF_5. In graphite at room temperature, the mobility is limited by phonon scattering, as it is in most metals.

The carbon and graphite fibers of interest here are not single crystals of graphite, but are made up of well defined graphite-like carbon planes oriented with their c-axis perpendicular to the fiber axis. Since they are made by pyrolysis of an organic precursor such as pitch or polyacrylonitrile (PAN), the degree to which the structure aproaches that of graphite depends upon the pyrolysis temperature (among other variables such as the precursor and its orientation). At low pyrolysis temperatures, there is little correlation between neighboring basal planes and the material is usually referred to as turbostratic. The crystallite sizes (as measured by x-ray diffraction) are small (20-200 Å) and the spacing between the basal planes is slightly larger than in graphite.

The resistance of graphite increases with increasing temperature because of the dominance of phonon scattering. Carbon and graphite fibers, on the other hand, have a decreasing resistance with increasing temperature because the dominant scattering mechanism is temperature independent boundary scattering. As the structure of the fibers becomes more like that of graphite, and the crystallite size grows, the temperature coefficient of resistance does not approach that of graphite, but becomes even more negative. (See Figure 1.)

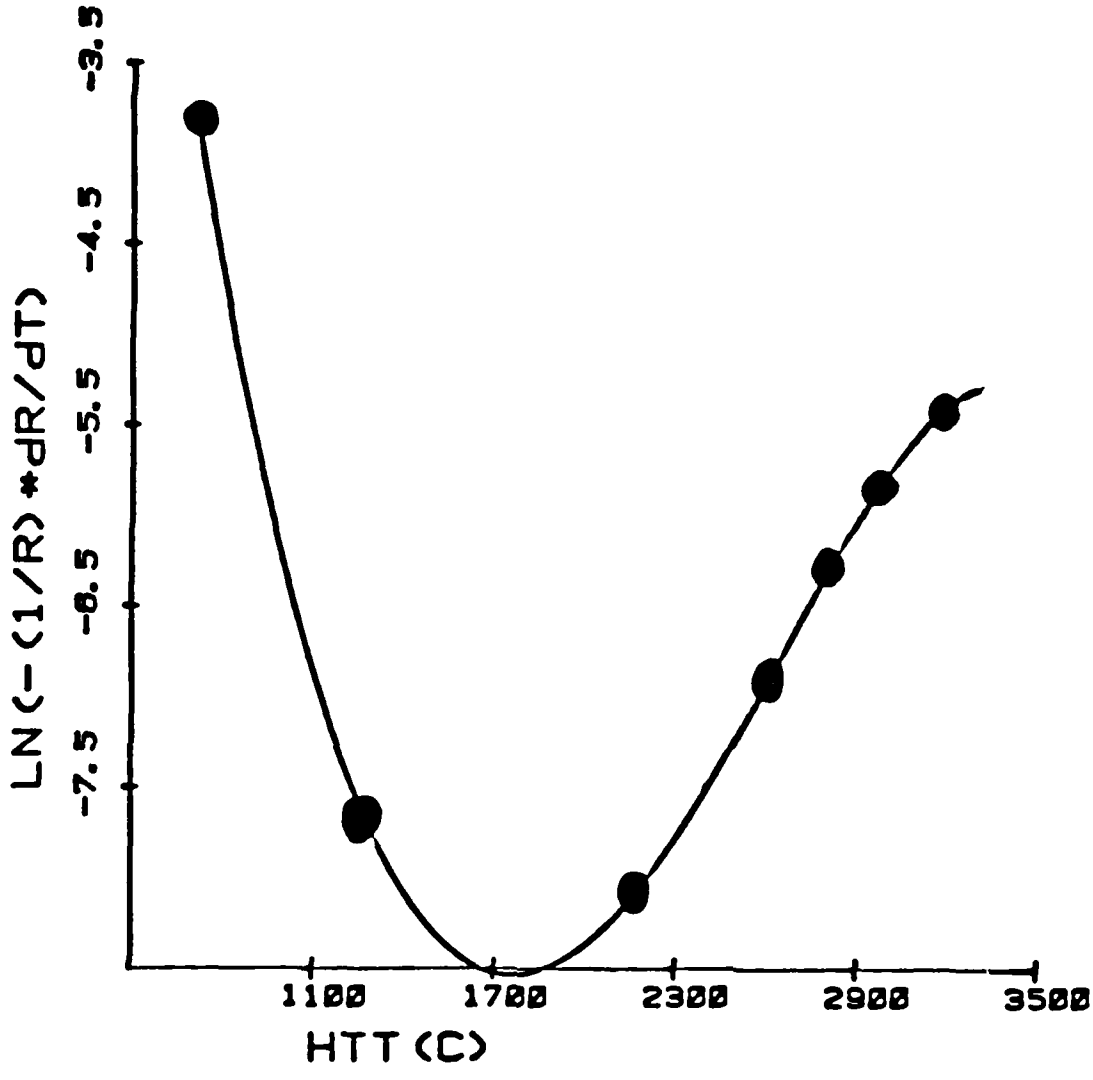

FIGURE 1. MAGNITUDE OF NEGATIVE TEMPERATURE COEFFICIENT OF RESISTANCE IN CARBON AND GRAPHITE FIBERS PLOTTED VS HEAT TREATMENT TEMPERATURE ON A LOG SCALE.

The simplifying assumption of a temperature independent mobility implies that the resistance versus temperature behavior is determined entirely by the temperature dependence of the carrier density. Using a simple two band model, we were able to estimate average band parameters (band overlap and fermi energy) for fibers. As shown in Table 1 (and discussed in more detail in Appendix I), the overlap is largest in the lowest modulus, most disordered, least graphitic fibers. This trend is model independent, since it is the overlap that sets the scale for the resistance change with temperature. Theories of the band structure of turbostratic graphite predict exactly the opposite behavior, i.e., a band gap for low heat treated fibers which decreases to zero as the crystallite size increases.

We can resolve this dilemma if we further utilize our simple model to estimate the fermi velocity and electron mean free paths in each fiber. The lifetime of the delocalized electron state responsible for the conduction of electricity across the crystallite can then be simply estimated as:

$$\tau \approx \frac{\lambda}{v_f}$$

where: τ is the lifetime
λ is the mean free path
v_f is the fermi viscosity

The results for the same set of ex-Pan fibers used in Appendix I are shown in Table 2. The decreasing overlap of the electron and hole states with increasing heat treatment can now be understood in terms of the energy uncertainty which results from the finite lifetime of the electrons within a single crystalite. As shown in Table 2, the energy uncertainty increases as we go to more

TABLE 1. PARAMETERS OBTAINED FROM SIMPLE TWO-BAND MODEL

Sample	HTT	ε_o(eV)	ε_F(eV)[1,2]	P(10^{24}/m^3)[3]	P(10^{18}/gm)[2]	v_f(10^6m/s)[2]	λÅ[2]
A	>3000	0.025	0.027	2.7	1.3	0.87	300
B	3000	0.029	0.031	3.2	1.5	0.94	230
C	2850	0.043	0.046	4.7	2.3	1.14	130
D	2700	0.052	0.053	5.4	2.8	1.23	100
E	2200	0.134	0.136	13.6	7.4	1.95	40

(1) From top of valence band.
(2) Assuming $m/m_o = 0.012$.
(3) P = hole density.

The parameters obtained from a fit of the simple two band model to Resistance vs Temperature data. The measured value of the resistivity was also used. The value of m/m_o was chosen to give a 40Å mean free path in fiber E. This value is consistent with effective masses commonly found in graphite.

TABLE 2. LIFETIME BROADENING

Fiber	ε_o(eV)	v_f(10^6m/s)	λÅ	τ(10^{-14}s)	ΔE(eV)
A	0.025	0.87	300	3.44	0.019
B	0.029	0.94	230	2.45	0.027
C	0.043	1.14	130	1.14	0.057
D	0.052	1.23	100	0.81	0.08
E	0.134	1.95	40	0.2	0.32

$\tau\Delta E = h/2\pi$

The lifetime of electrons in crystallites (τ) is calculated from the ratio of the electron mean free path (λ) to the electron fermi velocity (v_f). The uncertainty in the energy levels near the fermi level, E, is calculated from the Heisenberg Uncertainty Principle and is also shown. This result provides a simple explanation for the increasing overlap, ε_o, with decreasing modulus obtained from the resistance temperature data and the simple two-band model.

disordered fibers, and is comparable to or larger than the estimated overlap. Thus, even if an isolated basal plane has zero overlap or even a band gap, the short residence time for the electron on that plane broadens the energy levels and thus gives rise to a band overlap. Our model for the electronic properties of these fibers is one in which we have assumed that the conductivity is limited by the transit time across crystallites, and by the scattering which occurs at the boundary. As the transit time becomes shorter, one would expect to reach a point where the transition time between crystallites may limit the conductivity. Thus, one would have to model the conduction in the disordered regions of the fiber instead of the crystalline regions. This observation provides some insight into the anomolous resistance-temperature behavior of low modulus, high strength carbon fibers (see Appendix II). These fibers have a smaller crystallite size (by about a factor of 2) than the lowest modulus fiber listed in Tables 1 and 2 and thus intercrystallite transition rates may be more important. We still do not have an explanation for the resistance maximum in these fibers, but we do believe that it is related to the disorder at crystal boundaries.

IV. PIEZORESISTANCE OF CARBON AND GRAPHITE FIBERS

When a fiber is put under uniaxial stress, the fractional change in resistance per unit strain is called the piezoresistance. The most obvious reason for the existance of piezoresistance is that the geometry of the fiber changes. Earlier workers have also mentioned a number of other possible effects such as changes in orientation[11] and interparticle contact with stress.[6] We have assumed that these changes are less important than the changes in fiber geometry and the conductivity of the carbon planes. In order to understand these geometric effects fully, however, it is necessary to model both the piezoresistance, as well as to model the mechanical response of the fiber. Such modelling will require quantitative information on the micro-

structure. We have therefore broken this section into several parts. After discussing the theory of piezoresistance and of the mechanical properties, we describe the results of careful x-ray diffraction measurements on our fibers. We then describe the conclusions which can be reached thus far from our experiments. The importance of also doing hydrostatic pressure measurements is then discussed. Finally, the potential importance of effects not included in our simple models are reviewed.

1. Piezoresistance Theory:

We have divided the piezoresistance into three terms:

$$\frac{\Delta R}{R} = \varepsilon_{y'y'} - \left(\varepsilon_{x'x'} + \varepsilon_{z'z'}\right) - \varepsilon_{zz} \frac{\partial \ln \sigma}{\partial \varepsilon_{zz}}$$

where:

$\varepsilon_{y'y'}$ = the fractional increase in fiber length;

$\varepsilon_{x'x'} + \varepsilon_{z'z'}$ = the fractional increase in cross sectional area;

ε_{zz} = the fractional change in the basal plane separation.

One can therefore write:

$$\frac{\Delta R}{\varepsilon_{y'y'} R} = 1 - 2\nu + 7q\left[\frac{\varepsilon_{zz}}{\varepsilon_{y'y'}}\right]$$

where:

ν = Poisson's ratio (change in diameter/change in length).

The first two terms are just the change in resistance due to the change in fiber geometry with uniaxial strain. The third term represents what we feel will be the dominant change in conductivity for three dimensionally ordered graphite crystallites; the

increasing carrier density (and likewise increasing conductivity) as the basal planes are squeezed closer together. The factor of 7 in this term comes from the fact that the carrier density is proportional to the band overlap. In our simple model one expects the overlap to be about twice the absolute value of γ_2 (the interaction energy between carbon atoms on neighboring basal planes). The logarithmic derivative of γ_2 with respect to c-axis strain has been measured in single crystal graphite to be about 7.[12]

Since none of our fibers have complete stacking order (see Section IV-4, Figures 6a, 9, and Appendix III), we have multiplied the c-axis strain term by the factor q which will be between zero and one. If the entire carrier density were due to the band overlap caused by the interaction between carbon atoms in neighboring basal planes, and if the fiber had complete 3-dimensional stacking order as in graphite, then q would equal 1. Since it is clear from the x-ray diffraction that the stacking order is incomplete even in the most graphitic fibers, q will always be less than one and will go to zero for completely turbostratic materials. This effect will cause q to decrease with decreasing modulus. There are two other factors which will make q less than 1. As already discussed, a large part of the band overlap is probably caused by the lifetime broadening of the conduction electron energy levels. We saw that this was roughly equal to the overlap expected for graphite in the highest modulus ex-PAN fibers. In those fibers, we would therefore guess that q will be less than one half from this effect alone. Lower modulus fibers have even more overlap due to lifetime broadening resulting again in a lower q. Finally, we must remember that at room temperature many of the charge carriers are thermally excited. Within the simple two band model used, the number of thermally excited carriers is insensitive to the band overlap. In high modulus ex-PAN fibers at room temperature about half the carriers are thermally excited, thus reducing q by another factor of two.

This reduction will be smaller as the modulus gets smaller. Qualitatively we expect that low modulus fibers will have a positve piezoresistance dominated by the fractional increase in length and decrease in cross-sectional area. High modulus fibers will have an additional negative term in the piezoresistance since ε_{zz} will be negative (i.e. there will be compression along the c-axis) in most of the crystallites.

2. Theory of Mechanical Properties

In order to discuss the mechanical properties of these fibers, we again assume they are made up of graphite-like crystallites. Each crystallite will not have its c-axis exactly perpendicular to the fiber axis. This misorientation will be critical in determining the elastic properties. We have calculated the effective Young's modulus, Poisson ratio, and change in c-axis spacing for a crystal misoriented with respect to the fiber axis by an arbitrary amount. If we assume a uniform stress model for the fiber, the Young's modulus, Poisson ratio, and average change in c-axis spacing can be determined from the following equations:

$$\frac{\varepsilon_{y'y'}}{\sigma_{y'y'}} = Y^{-1} = S_{11}(1-w^2)^2 + (2S_{13}+S_{44})w^2(1-w^2) + S_{33}w^4$$

$$\frac{\varepsilon_{x'x'}+\varepsilon_{z'z'}}{\sigma_{y'y'}} = \frac{2\nu}{Y} =$$

$$(S_{11}+S_{33}-S_{44})w^2(1-w^2) + S_{13}(2w^4-w^2+1) + S_{12}(1-w^2)$$

$$\frac{\varepsilon_{zz}}{\sigma_{y'y'}} = S_{13}(1-w^2) + S_{33}w^2$$

$$w^2 = \langle\sin^2\theta\rangle \qquad w^4 = \langle\sin^4\theta\rangle$$

The average values of $\sin^2\theta$ and $\sin^4\theta$ can be obtained from x-ray diffraction as will be discussed later.

One of the major problems with this approach is that one needs to know the elastic constants of the crystallites. Although S_{11} and S_{12} should be close to their single crystal value (see Table 3), it is well known that S_{44} is sensitive to defects and disorder.[12] In addition, the value for S_{13} in graphite is still uncertain, with the usually accepted value being -0.33E-12/Pa. However, thermal expansion data indicates that a value as large as -1.8E-12/Pa may be correct for single crystals. We have therefore calculated the three properties of interest to the piezoresistance for a range of choices of S_{44} and S_{13}. The single crystal values were used for the remaining elastic constants. The results are shown in Figures 2-4. Young's Modulus depends primarily on orientation and S_{44} and is not strongly dependent on S_{13}. The Poisson ratio and c-axis strain depend primarily on S_{13} for well oriented fibers, and on S_{44} for poorly oriented fibers.

Our approach has been to use the measured value of Young's modulus to determine the value of S_{44}. This requires an accurate determination of the crystallite orientation distribution. Therefore, we will discuss this measurement before proceeding further.

3. Orientation

The orientation distribution of the graphite basal planes can be determined directly from any (002) diffraction line (see Figures 5a and b). The average values of $\sin^2\theta$ and $\sin^4\theta$ can be calculated from the data, although these averages are extremely sensitive to the tails of the distribution. Most researchers[24] have assumed a functional form for the distribution such as:

$$I(\theta) = \cos^n\theta$$

TABLE 3. ELASTIC CONSTANTS OF GRAPHITE CRYSTALS[1]

Elastic Moduli ($\times 10^{10}$ Pa)		Elastic Compliance ($\times 10^{-12}$ Pa^{-1})	
C_{11}	1.06	S_{11}	0.98
C_{12}	0.18	S_{12}	-0.16
C_{13}	0.015	S_{13}	-0.33, -1.8[2]
C_{33}	0.0365	S_{33}	27.5
C_{44}	0.0045	S_{44}	240

(1) From ref 12.
(2) From thermal expansion data.

The accepted values of the elastic constant of single-crystal graphite are shown. The value of S_{13} is uncertain, and two values obtained from different experiments are given.

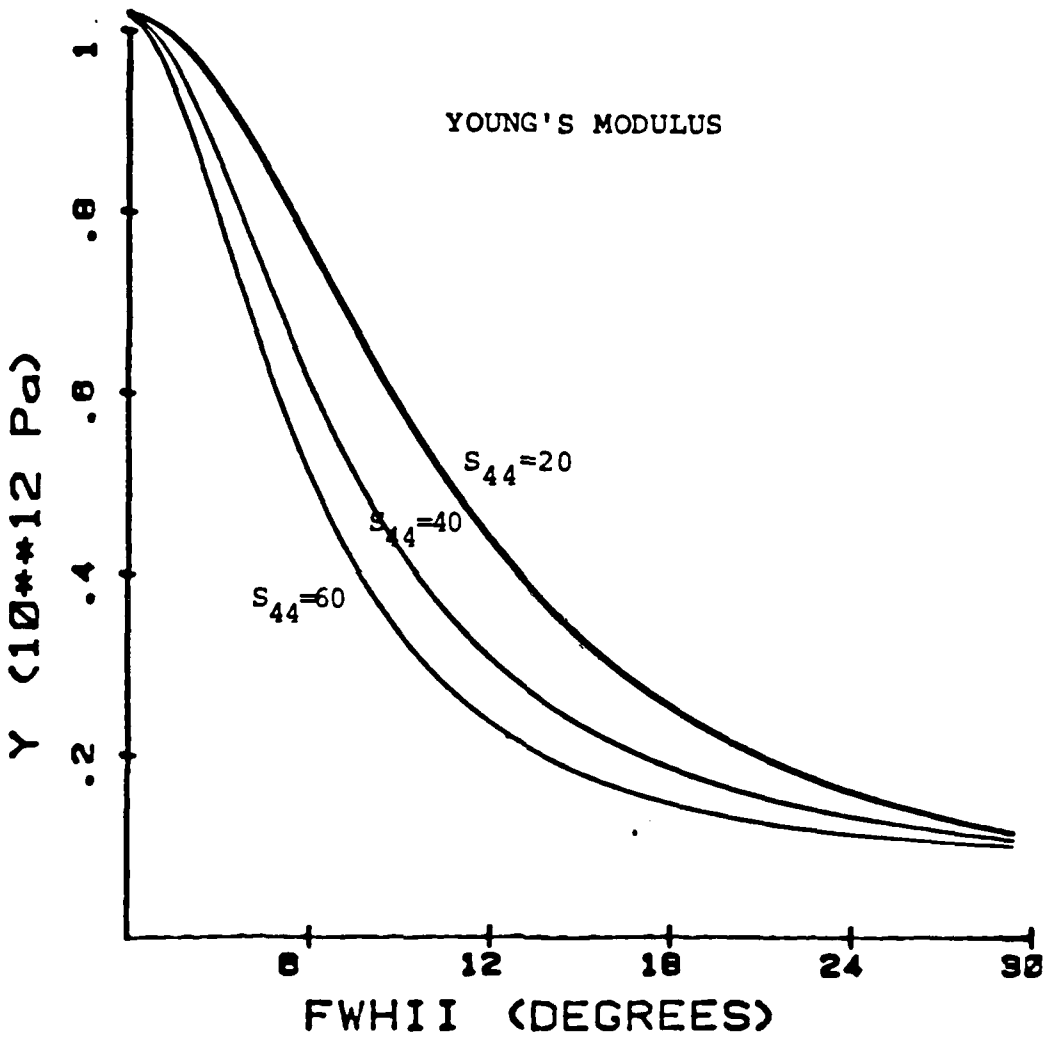

FIGURE 2. A CALCULATION OF YOUNG'S MODULUS VERSUS CRYSTALLITE ORIENTATION IS SHOWN FOR VARIOUS CHOICES OF S_{44}.

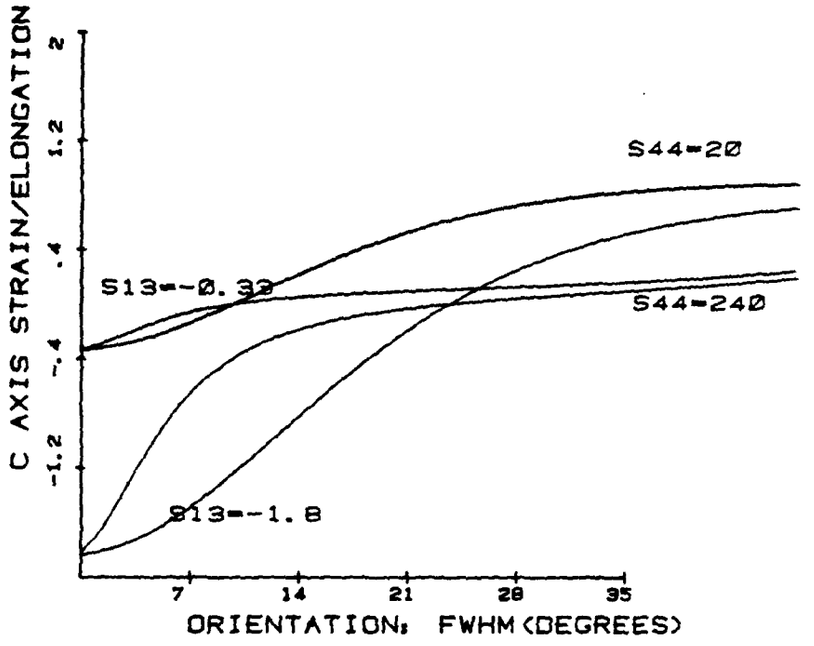

FIGURE 3. POISSON RATIO VERSUS ORIENTATION CALCULATED FOR: S_{13} = -0.33 and -1.8 x 10^{-12}/Pa; S_{44} = 20 and 240 x 10^{-12}/Pa.

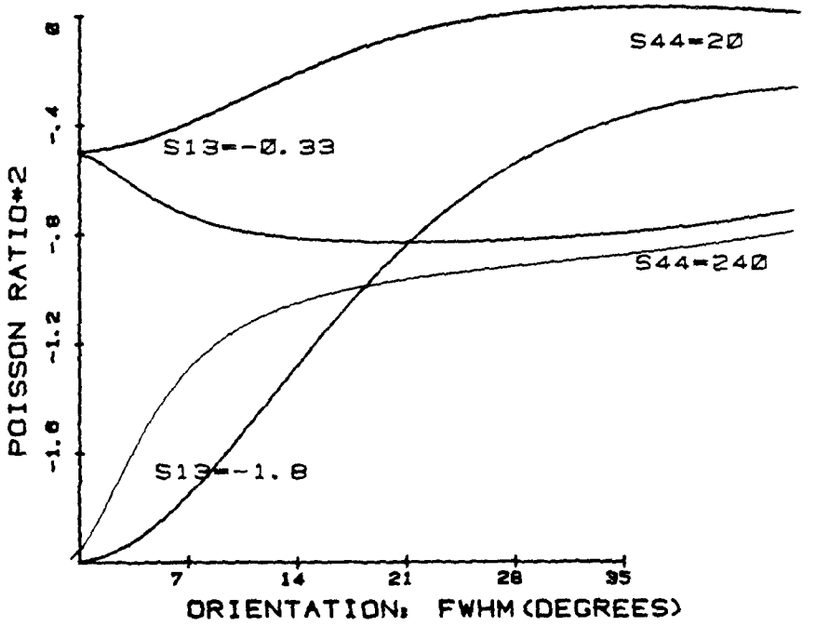

FIGURE 4. THE RATIO OF C-AXIS STRAIN TO ELONGATION VERSUS ORIENTATION FOR S_{13} = -0.33 and -1.8 x 10^{-12}/Pa; S_{44} = 20 and 240 x 10^{-12}/Pa.

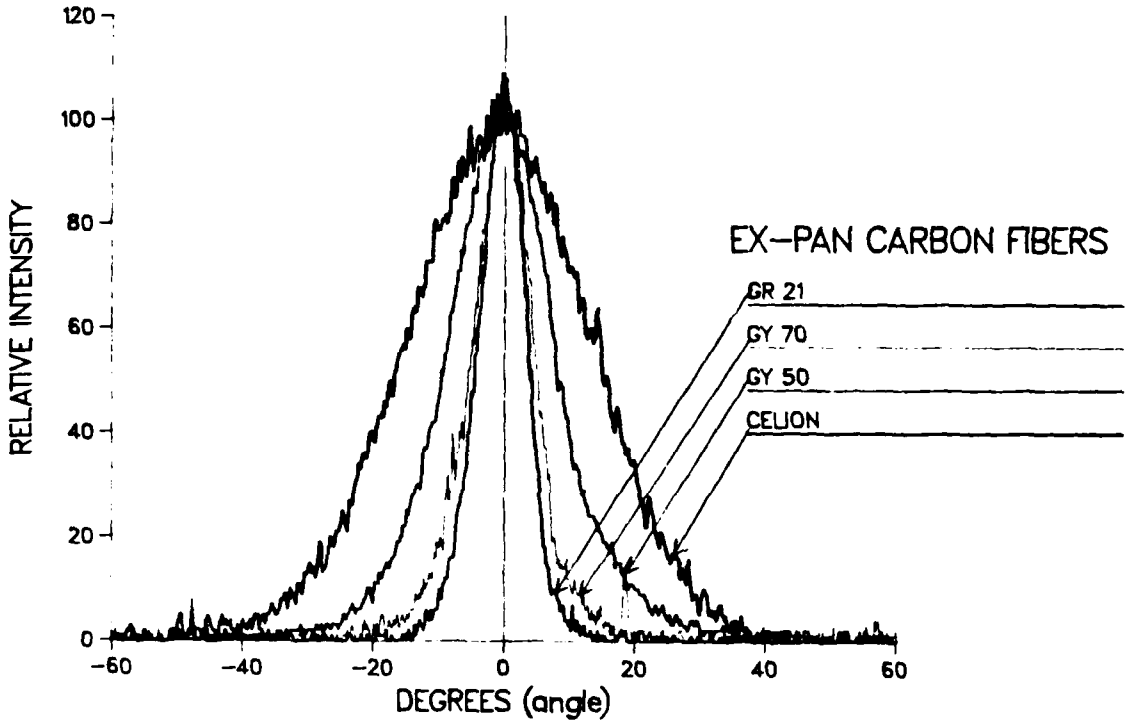

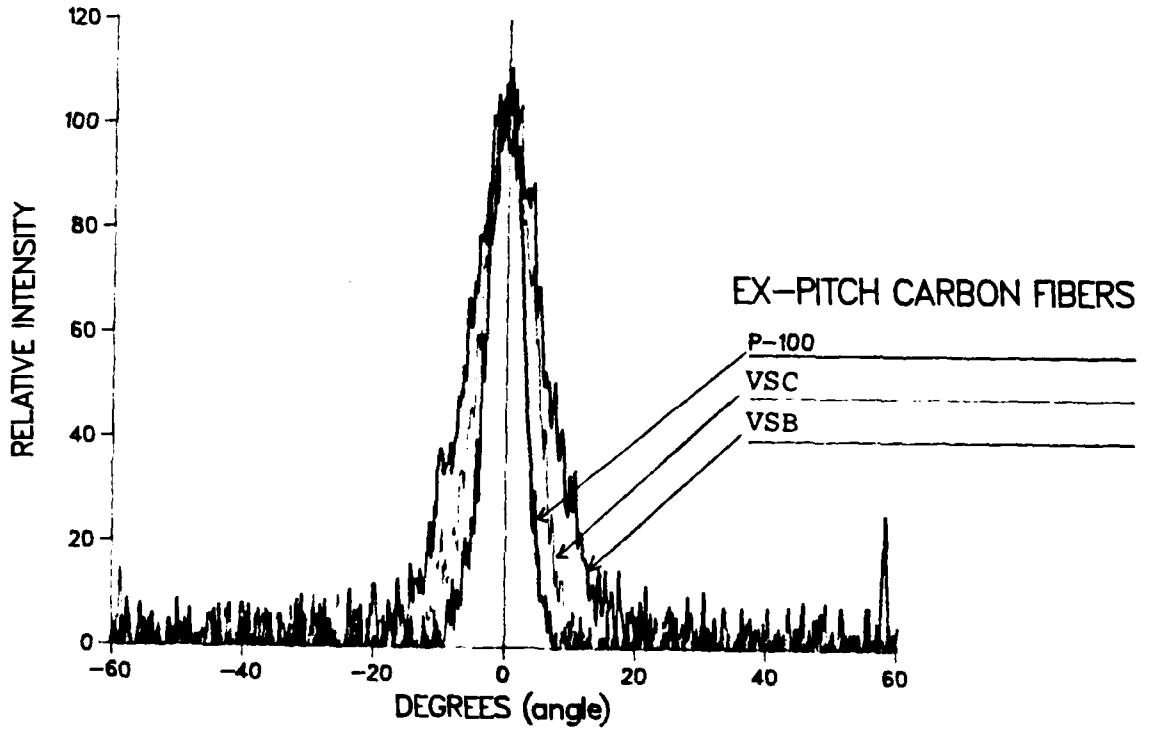

FIGURE 5 (a & b) THE 002 ROCKING CURVES ARE SHOWN FOR THE EX-PAN AND EX-PITCH FIBERS. THE MOST ORIENTED CURVES ARE FOR THE HIGHER MODULUS FIBERS. THESE DATA WERE USED TO CALCULATE THE VALUES OF $\langle \sin^2\theta \rangle$ AND $\langle \sin^4\theta \rangle$ NEEDED FOR MODELLING THE ELASTIC PROPERTIES.

The average values can then be determined simply by measuring the full width at half maximum (FWHM) or full width at half integral intensity (FWHII), determining the value of n, and then calculating the integrals analytically. For the above described distribution, the FWHM and FWHII are almost equal. However, these values are very different in all the x-ray patterns we have checked thus far. This implies the above choice is probably not an accurate representaion of the distribution function. A Gaussian distribution has FWHM=1.74 x FWHII which is closer to what we observe (see Table 4). The values of $\langle \sin^2(\theta) \rangle$ calculated directly from the x-ray data are in reasonable agreement with those calculated from the value of the FWHII and assuming a Gaussian distribution.

We used $\langle \sin^2\theta \rangle$ calculated directly from the distribution function to calculate the effective elastic constants and c-axis strain (see Table 5). Because of the uncertainty in the value of the elastic constants, we have used the measured value of Young's modulus (Y) for each fiber, and single crystal values for all elastic constants except S_{44} in order to determine an effective S_{44}.

The calculated values of S_{44} are much lower than the single crystal value of 240E-12/Pa. The low value is expected from the high defect concentrations in these materials. Given the large number of uncertainties in this calculation, only the following qualitative trends are considered significant:

(1) Very high modulus fibers (GR-21 and P-100) have lower values of S_{44} than lower modulus fibers. This is consistent with earlier observations that the torsional modulus of fibers decreases at high values of Young's modulus.[13] It is also in agreement with a similar analysis by Reynolds.[14] It is opposite to what one might expect based upon the increasing three dimensional order of these fibers. At present, we have no explanation for this effect.

TABLE 4. MISORIENTATION DISTRIBUTION

Fiber	θ (FWHM)	θ (FWHII)	Ratio
Celion	32.5	20.6	1.6
G-50	17.6	11.4	1.5
GY-70	10.8	7.5	1.4
GR-21	9.4	5.8	1.6
VSB	13.5	8.0	1.7
VSC	10.4	5.9	1.8
P-100	7.1	4.0	1.8

The full width at half maximum (FWHM), the full width at half integral intensity (FWHII), and their ratio are shown for both ex-PAN and ex-Pitch Fibers. The ratio would be 1.7 for a Gaussian distribution, and near 1 for a $\cos^{n}\theta$ distribution.

TABLE 5. S_{44} FROM YOUNG'S MODULUS

Fiber	Y(E12Pa)	θ (FWHII)	S_{44} (E-12/Pa)
Celion	0.37	20.6	18.6
G-50	0.56	11.4	22.4
GY-70	0.73	7.5	18.8
GR-21	0.93	5.8	12.2
VSB	0.45	8.0	66
VSC	0.66	5.9	54
P-100	0.96	3.6	21

(2) Pitch fibers have larger values of S_{44} than ex-PAN fibers of similar modulus. This can be understood in terms of the lower number of defects in ex-pitch fibers which tie basal planes together. Pitch fibers are more three dimensionally ordered than ex-PAN fibers, thus implying that the changes in S_{44} are not correlated with stacking order.

(3) As the modulus increases, the Poisson ratio also increases. This is simply a consequence of the increasing orientational order in the fibers.

4. Three-Dimensional Order

As discussed in Appendix III, carbon fibers have a gradually improving correlation of atoms in neighboring basal planes with increasing heat treatment. This means that the structure is getting closer to that of graphite, and that interplane interactions are becoming more important to the electrical properties. The parameter, q, which was defined earlier, is a measure of the importance of interplane interactions.

Figures 6a-g show 11ℓ diffraction scans on 4 ex-PAN fibers and 3 ex-Pitch fibers. The width of the 110 line is due both to in plane crystallite size and to the lack of 3-dimensional order. As one goes to higher modulus fibers, the 110 line sharpens and a distinct 112 line appears. This means that there are long range correlations in the position of carbon atoms on different basal planes. The diffraction pattern is still very different from fully crystalline graphite, since in graphite the ratio of the 112 intensity would be larger than the 110 intensity.

5. Results From Piezoresistance

As can be seen from Figures 7 and 8, the measured piezoresistance of low modulus fibers is positive and that of high modu-

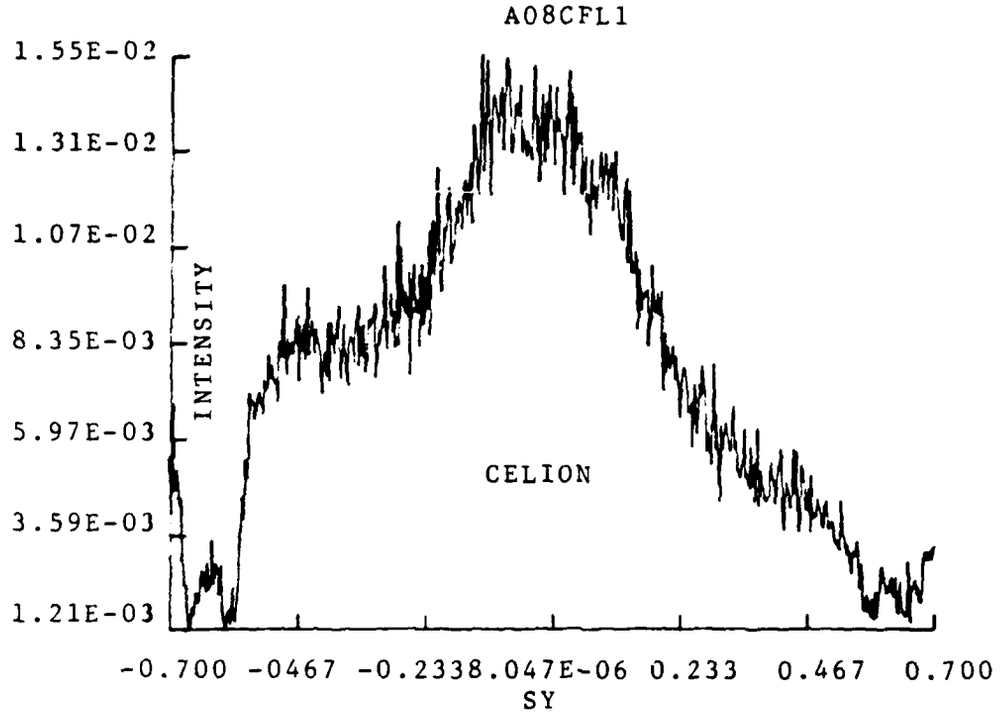

a. CELION

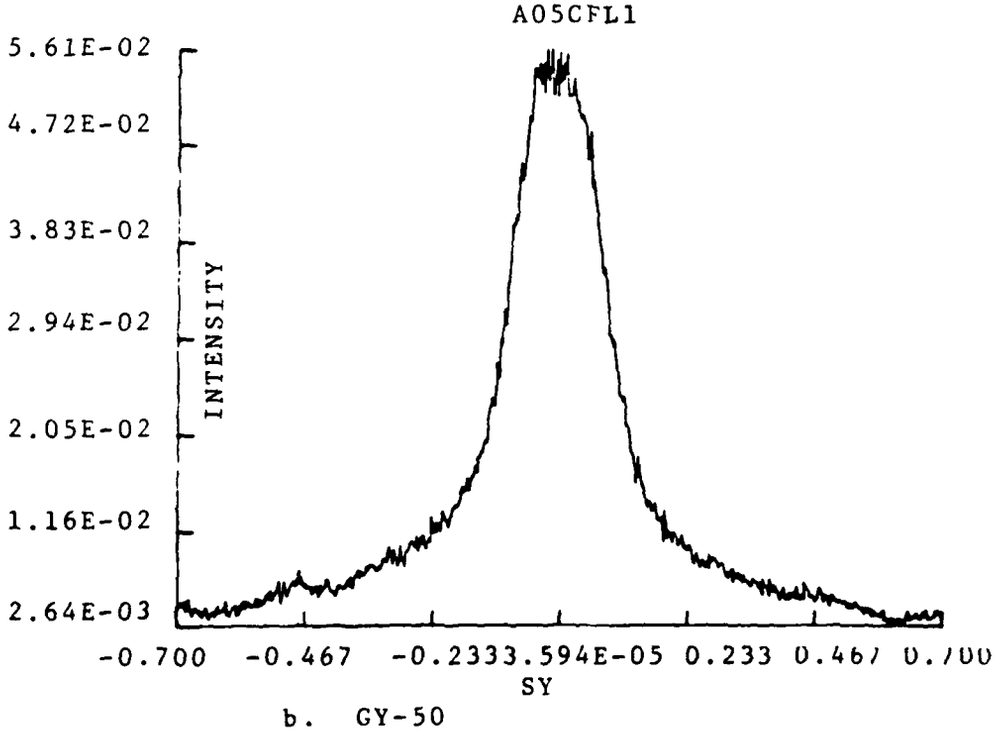

b. GY-50

FIGURE 6. 11ℓ DIFFRACTION SCANS OF EX-PAN AND EX-PITCH FIBERS

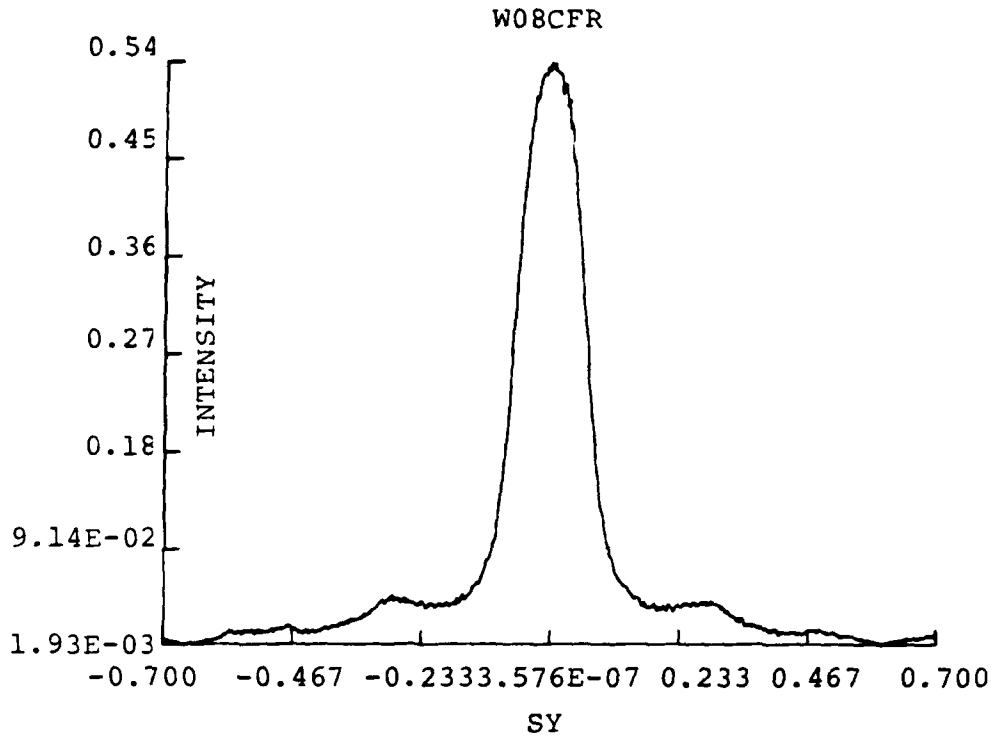

c. GY-70

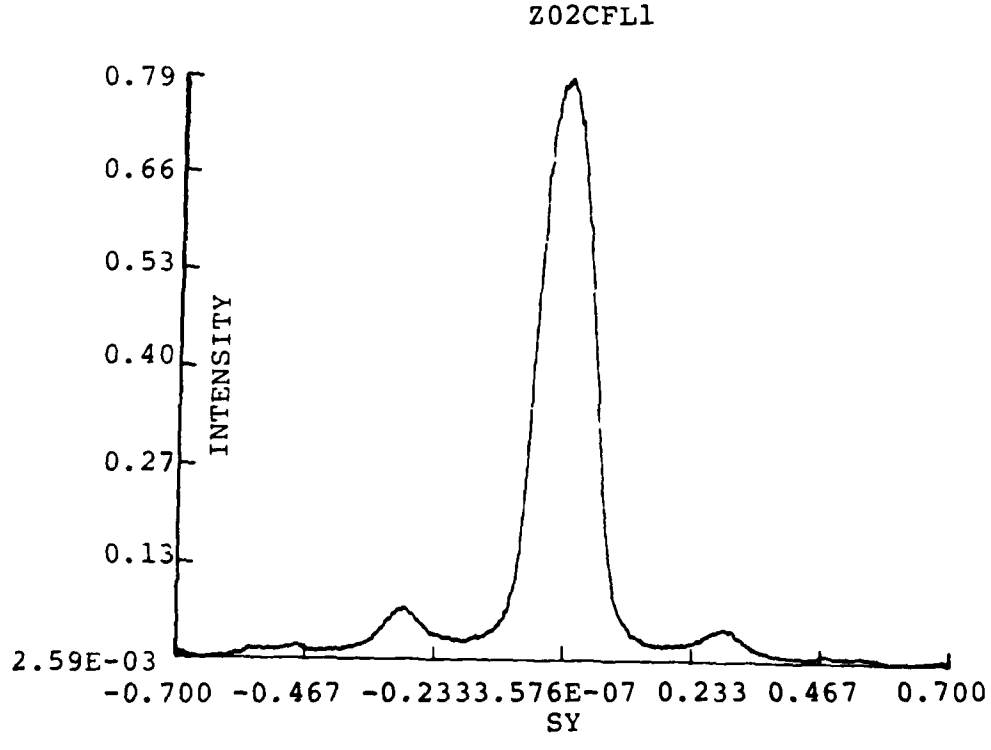

d. GR-21

FIGURE 6. 11ℓ DIFFRACTION SCANS OF EX-PAN AND EX-PITCH FIBERS

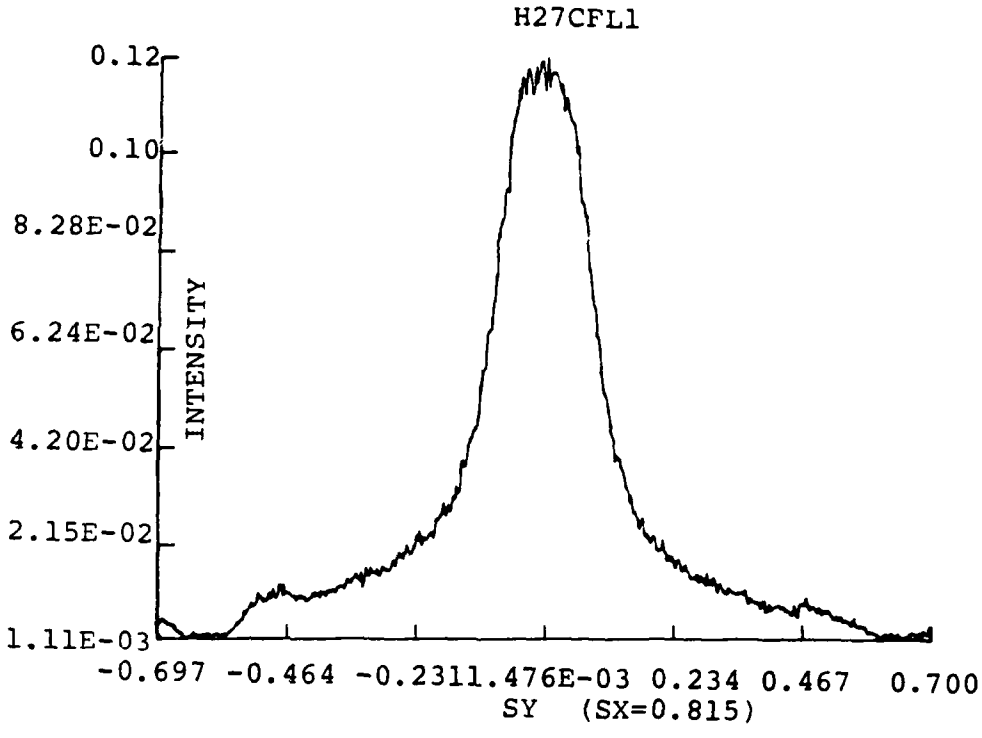

e. VSB

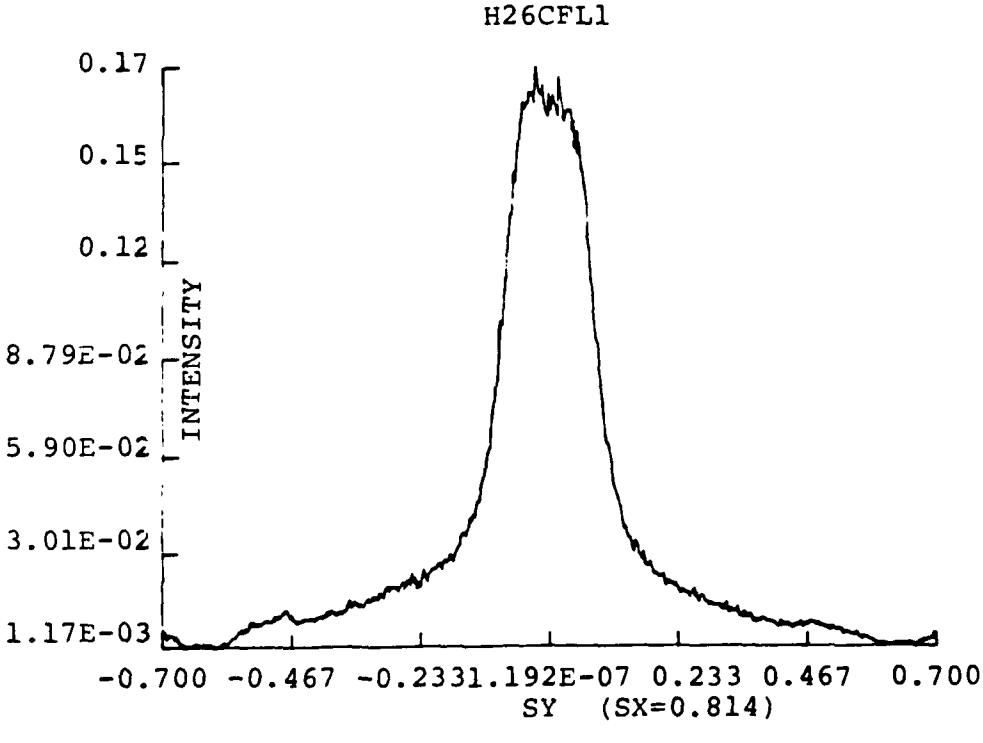

f. VSC

FIGURE 6. 11ℓ DIFFRACTION SCANS OF EX-PAN AND EX-PITCH FIBERS

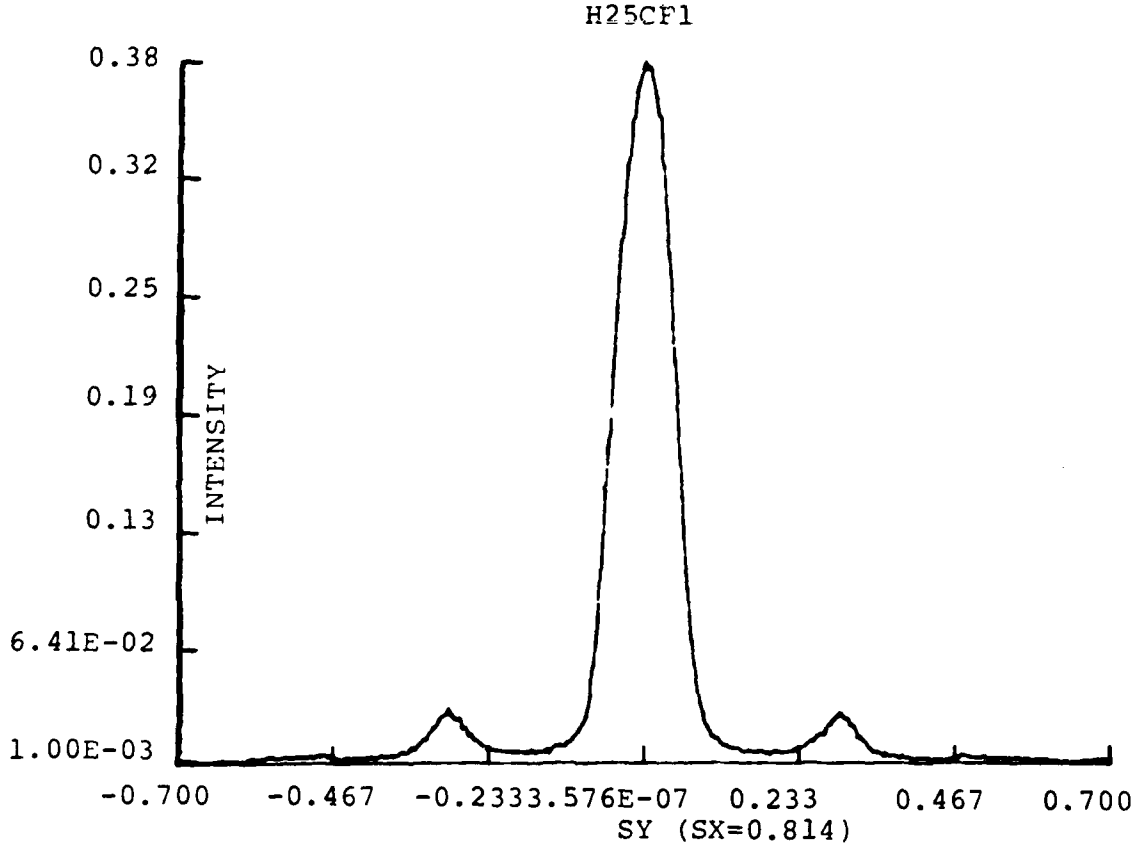

g. P-100

FIGURE 6. 11ℓ DIFFRACTION SCANS OF EX-PAN AND EX-PITCH FIBERS

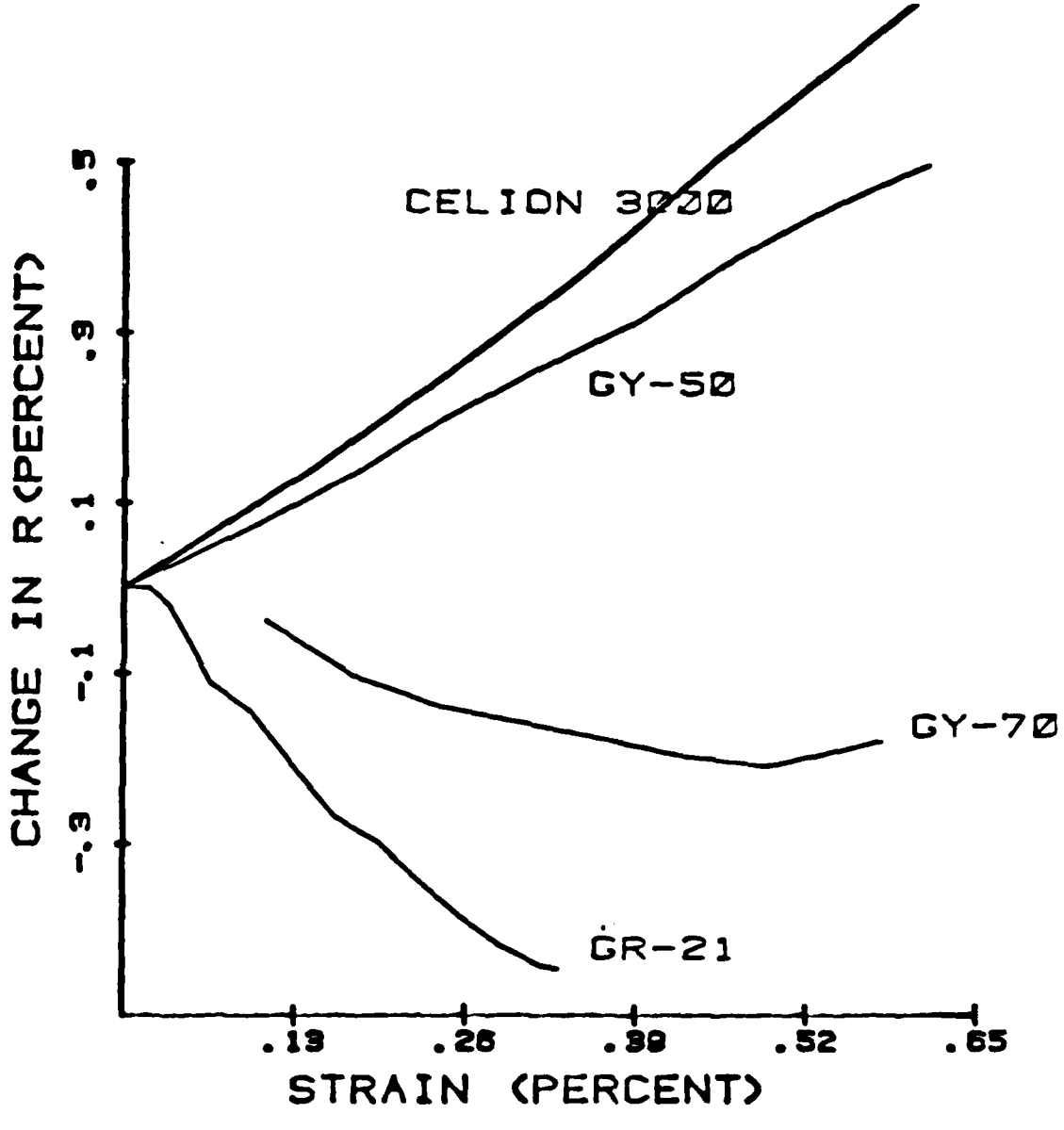

FIGURE 7. PIEZORESISTANCE OF EX-PAN FIBERS

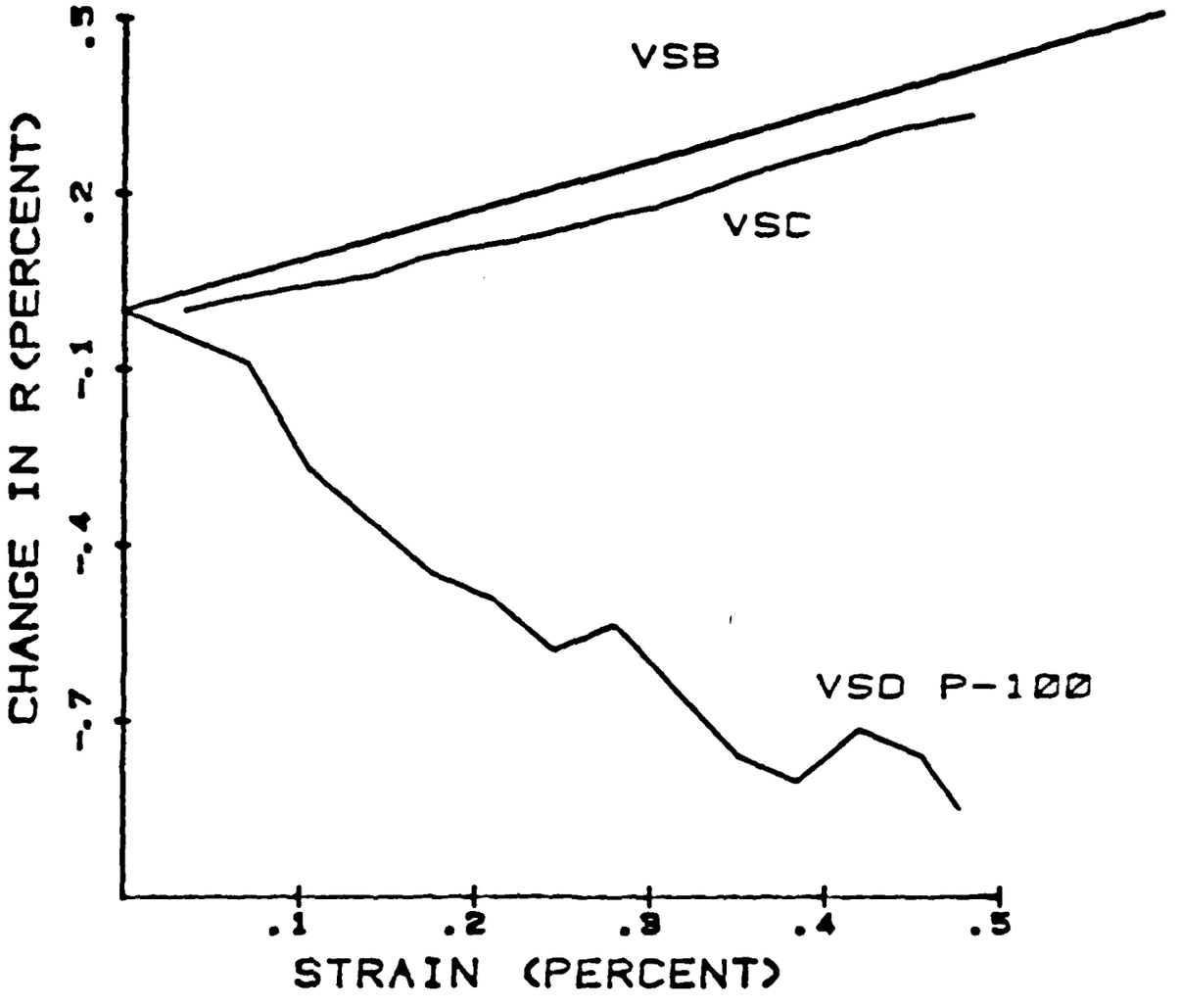

FIGURE 8. PIEZORESISTANCE OF EX-PITCH FIBERS

lus fibers is negative, as expected. In Figures 9a-e, we show our calculation of the piezoresistance in two limits:

(1) no change in carrier density with strain -- labelled 2-D since this is what we expect for a completely turbostratic fiber (i.e., q=0);

(2) the change in carrier density given by that expected for single crystal graphite at low temperatures under the same average strain along the c axis (i.e., q=1).

Of course we are still assuming (as we have throughout) that changes in conductivity only occur because of changes in carrier density on the basal planes. Notice that whenever S_{13}=-1.8E-12/Pa the experimentally determined piezoresistance falls between our two theoretical limits. When S_{13}=-0.33E-12/Pa much of the data falls outside the range expected in our model. The error bars on the data are primarily due to the fact that many samples have a non-linear piezoresistance. The place where the 2-D and 3-D limits cross is where there is no change in the average interplanar spacing. It is interesting to note that those fibers exhibiting negative piezoresistance also showed the most non-linear piezoresistance, while those near the place where the average c-axis strain is zero (for small values of S_{44}) had the most linear piezoresistance.

When S_{44} is chosen close to the values obtained from Young's modulus and the measured values of $\sin^2\theta$, the high modulus fibers have negative piezoresistance remarkably close to the 3-D limit. However, when a larger value of S_{44} is used, the fibers will have a small value of q consistent with our earlier discussion. This may imply that other mechanisms are also important to the piezoresistance, or that our model for the elastic constants should be improved. These points will be discussed in Part 7.

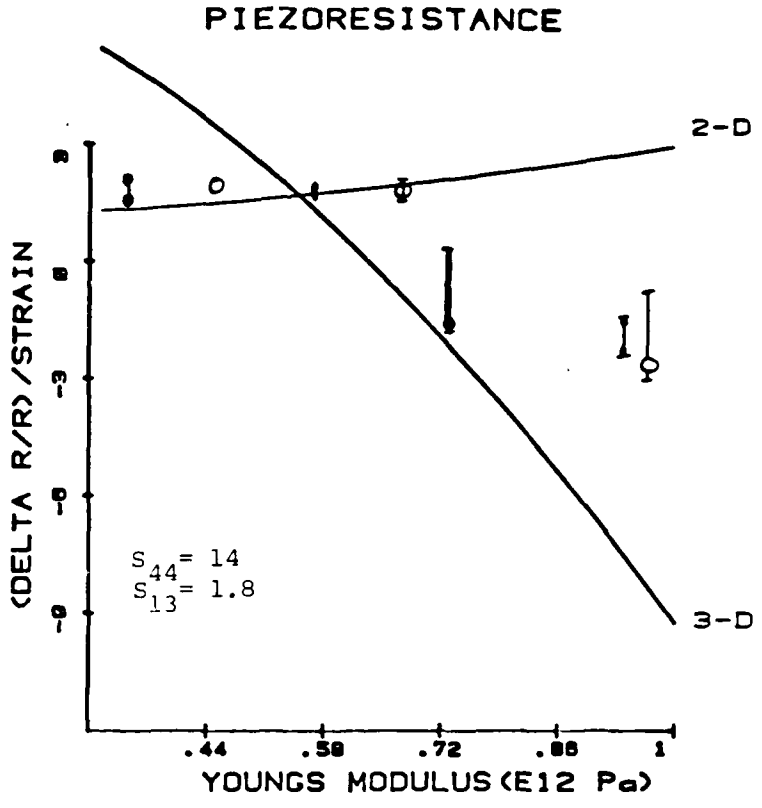

a.

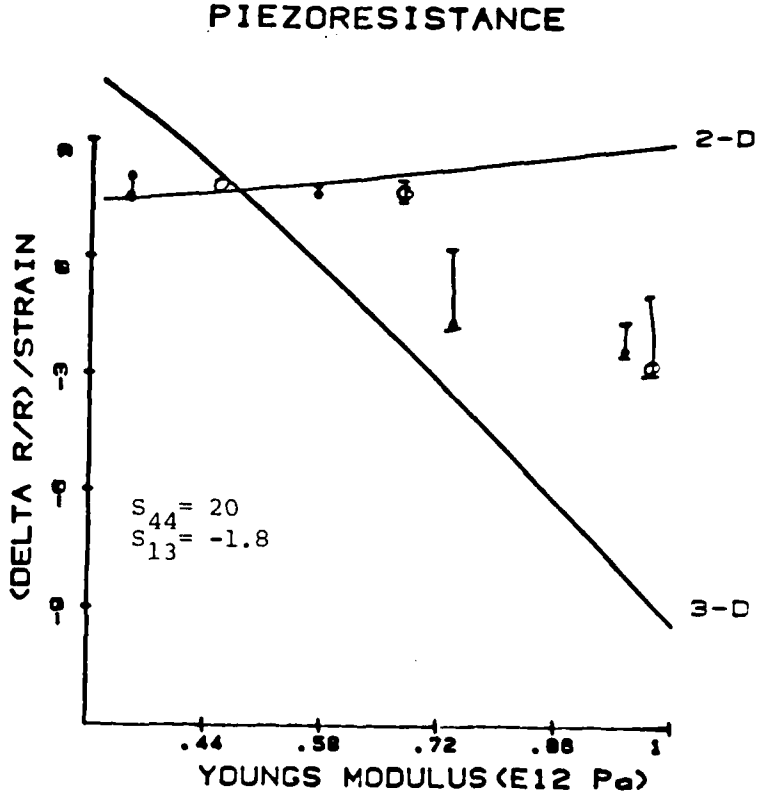

b.

FIGURE 9. PIEZORESISTANCE VERSUS YOUNG'S MODULUS

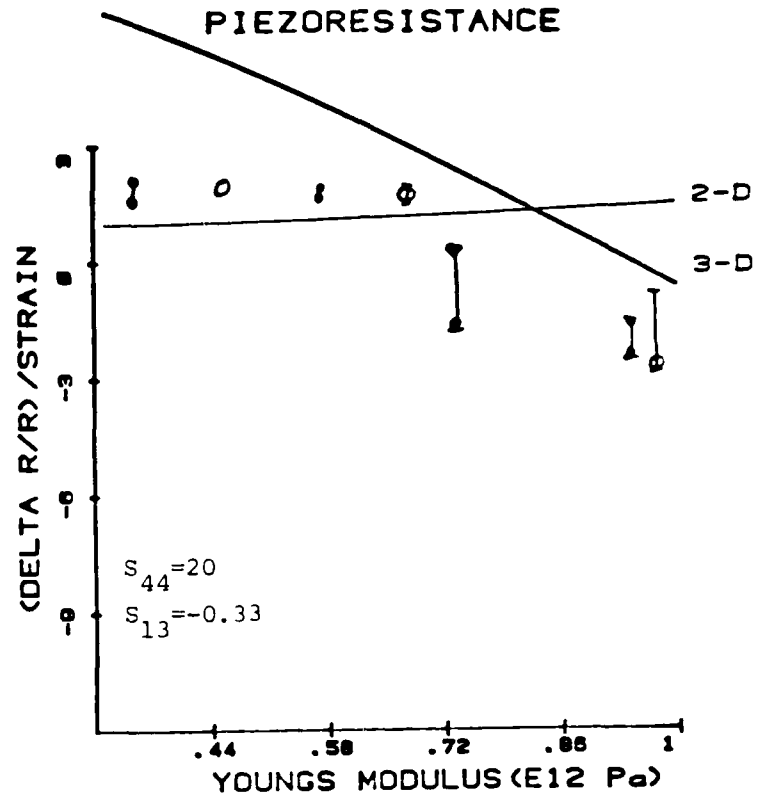

c.

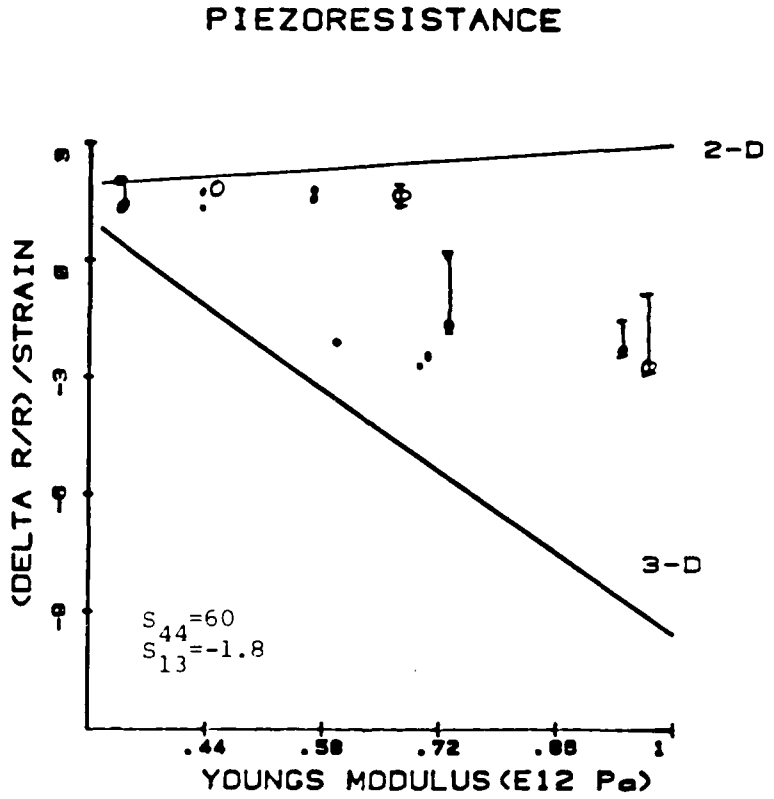

d.

FIGURE 9. PIEZORESISTANCE VERSUS YOUNG'S MODULUS

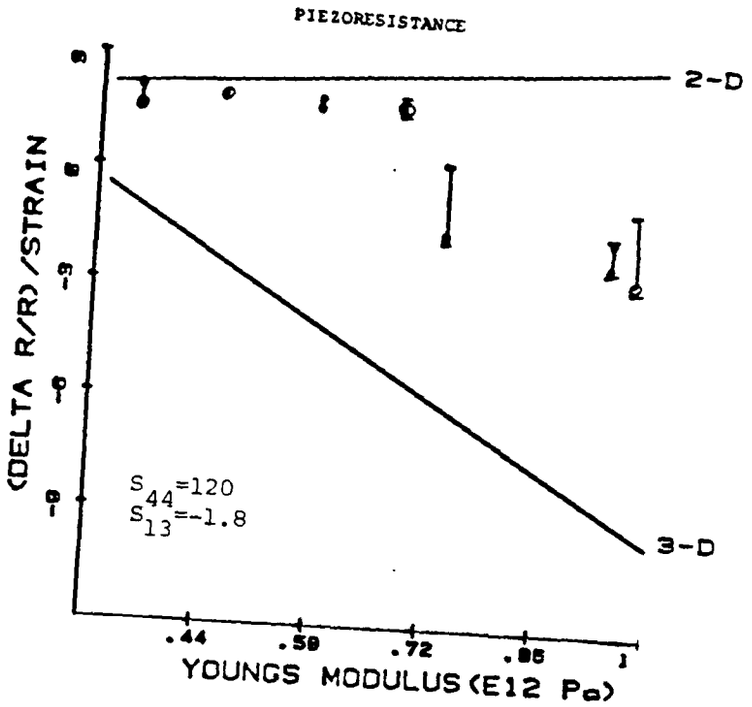

e.

FIGURE 9. PIEZORESISTANCE VERSUS YOUNG'S MODULUS

We show the first measurement of piezoresistance in an intercalated fiber in Figure 10. The fiber was a mixture of stage 1 and stage 2 $CuCl_2$-intercalated graphite, with some unintercalated graphite still observable in x-ray diffraction. The resistance was about 20 times lower than the unintercalated P-100 fibers from which the sample was made. Suprisingly, the piezoresistance is negative. This implies that the charge transfer in this compound depends upon c-axis strain. The data shown in Figure 10 is from one of two measurements made thus far. Both gave very similar results.

6. Hydrostatic Pressure Experiments

The considerable uncertainty in the elastic constants of the graphite crystallites makes detailed analysis of piezoresistance difficult. There are two ways in which we are trying to eliminate these uncertainties. One is to measure the c-axis compression directly during uniaxial stress. Since it is difficult to assure that all filaments in a bundle have the same stress, it will be necessary to do this work on single filaments. This would also have to be coupled with an accurate determination of the orientation distribution, preferably also done on the same single filament. Given the difficulties in accurately measuring the tails of the distribution on small bundles of fibers, such work on single filaments will be extremely time consuming.

A more promising approach is to measure the changes in fiber properties with hydrostatic pressure. Unlike the case of uniaxial stress, it is straightforward to apply an equal hydrostatic pressure to many filaments at once. A direct determination of the change in c-axis spacing with hrydrostatic pressure will primarily determine the sum: $S_{33}+2S_{13}$. As summarized in Table 6, the change in resistance with hydrostatic pressure is determined by the same sum of elastic constants, and of course by the factor

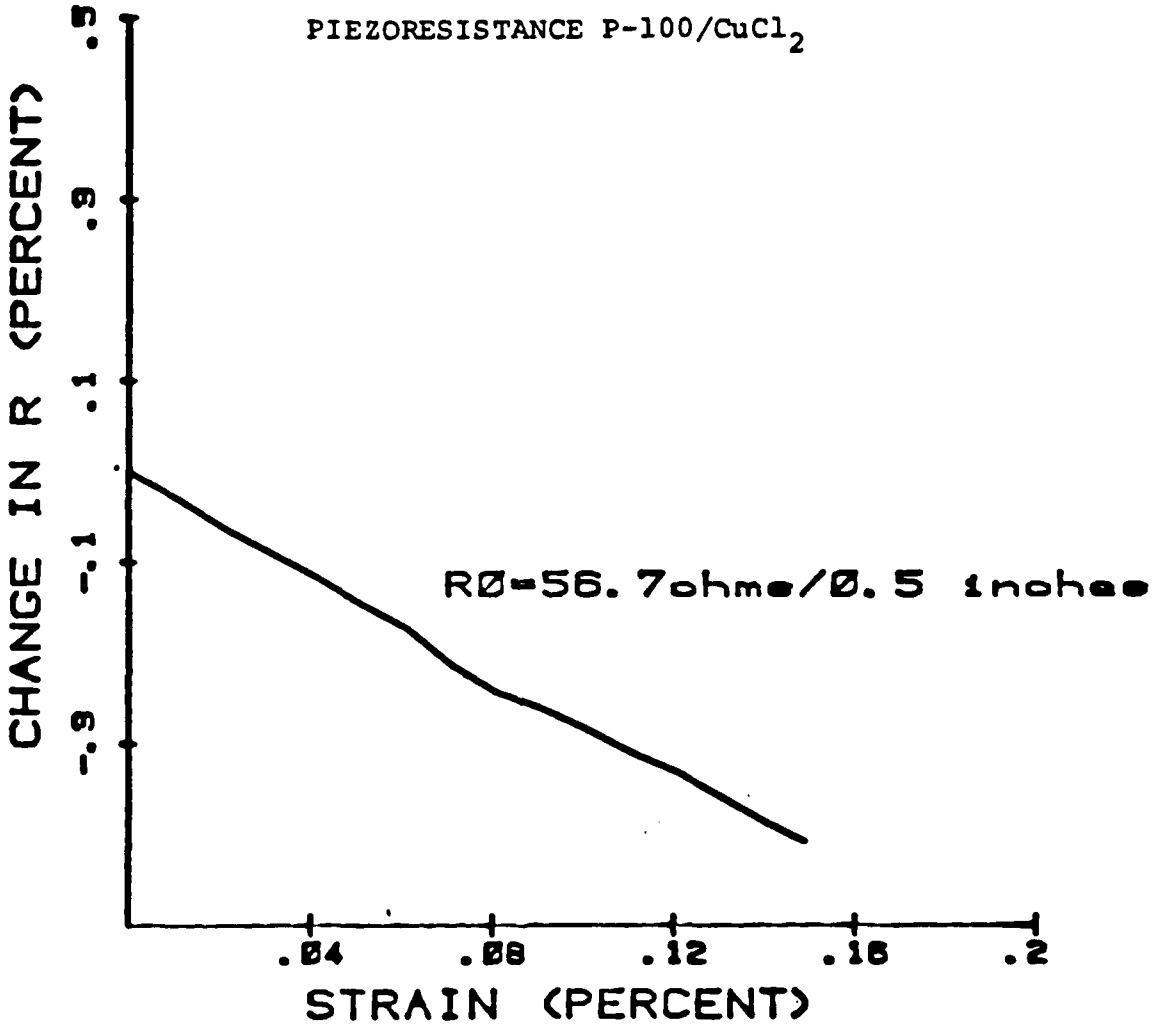

FIGURE 10. PIEZORESISTANCE OF $CuCl_2$ INTERCALATED FIBER

TABLE 6. HYDROSTATIC PRESSURE

$w = \sin\theta$

$$\varepsilon y'y' = -\frac{P}{3}\left[(1-\langle w^2\rangle)(S_{11}+S_{12}+S_{13})+\langle w^2\rangle(2S_{13}+S_{33})\right]$$

$$\varepsilon x'x' + \varepsilon z'z' = -\frac{P}{3}\left[(1+\langle w^2\rangle)(S_{11}+S_{12}+S_{13})+(1-\langle w^2\rangle(2S_{13}+S_{33})\right]$$

$$\varepsilon zz = -\frac{P}{3}\left[2S_{13}+S_{33}\right]$$

2-D R Change with P

$$\frac{1}{P}\frac{\Delta R}{R} = \frac{1}{3}\left[(1-2\langle w^2\rangle)(2S_{13}+S_{33})+2\langle w^2\rangle(S_{11}+S_{12}+S_{13})\right]$$

which for well oriented fibers gives

$$\frac{1}{P}\frac{\Delta R}{R} \sim \frac{1}{3}(2S_{13}+S_{33})$$

3-D R Change with P

$$\frac{1}{P}\frac{\Delta R}{R} = \frac{1}{3}(2S_{13}+S_{33})(1-7q)$$

q defined previously. Thus, in addition to more information about the elastic constants of the fibers, one would have a fairly direct determination of q. This would provide the best test of our model. These measurements are in progress.

Recently, Fischbach[15] reported that low modulus fibers show a decrease in resistance with increasing hydrostatic pressure while high modulus fibers show a very small increase in resistance. The decrease observed in the low modulus fibers may be due to changes in interparticle contacts in the fibers. Preliminary results by I. Spain indicate that the resistance of low modulus[16] fibers decrease under oil pressure, but not under gas pressure. The gas can presumably penetrate the porosity of the low modulus fibers, and thus does not change intercrystalline contacts as much as oil pressure. The high modulus fibers studied by Fischbach presumably have a small amount of 3-D order. These fibers were not characterized by x-ray diffraction, so it is difficult to say how they compare with the samples looked at in our work.

7. Other Effects

We have concentrated on what we feel are the two simplest effects of stress on resistance in carbon and graphite fibers. Most other work on piezoresistance has concentrated on the unwrinkling ribbon model of Ruland.[17] In that model, Young's modulus is determined not soley by the orientation of crystallites, but also by their ability to reorient under stress. This effect has been observed both in x-ray diffraction[11] and in measurements in the changes in Young's modulus with increasing strain. Beetz[18] has found, for example that the change in Young's modulus with increasing strain is larger in pitch fibers than in PAN fibers. Such effects would have to be included in a complete quantitative theory of piezoresistance. An increasing orienta-

tion with strain would reduce the positive term in the piezoresistance from geometric changes, since the effective path length electrons would not increase even though the length would. In addition, the compression along the c-axis of the crystallites would increase as the orientation improves. These two effects would combine to make the predictions of our model more negative and may be an explanation for the piezoresistance being so close to the 3-D (i.e., q near 1). In addition, such effects could explain the non-linear nature of piezoresistance in some of the fibers (particularly those of intermediate modulus like GY-70), since the expected piezoresistance is extremely sensitive to our choice of crystalline elastic constants. These could also be changing with orientation.

Another effect neglected in our model is the effect of defects and disorder on the piezoresistance. It is expected that defects control the position of the fermi level with respect to the band edges, and thus the carrier concentration. If the charge transfer to these defects depends upon the strain, one would expect additional contributions to the resistance changes. It is our belief that a complete theory based on the simple model used here, but incorporating a larger number of mechanical and electrical characterizations, and including changes in orientation and elastic constants with stress, would be particularly valuable in elucidating the role and nature of defects in carbon and graphite fibers. For example, if the primary defects contributing to the electron density were interstitial carbon atoms between basal planes, one would expect them to have an increasing charge transfer with decreasing distance between the basal planes. This could be another source of negative piezoresistance in high modulus fibers, and an extra source of positive piezoresistance in low modulus fibers.

It is important to remember that our electrical and elastic models are based on the properties of the small crystallites making up the fibers. The difficulties in making an accurate description of the electrical properties based on the properties of isolated crystallites are already evident from our need to invoke the Heisenberg uncertainty relationship in order to explain the average properties of the fibers. The problems involved in determining the elastic properties of a collection of anisotropic crystallites from the properties of the constituents is even more difficult. Price[19] has shown that a uniform stress model is useful in explaining Young's modulus in a number of graphitic materials with differing degrees of orientation. Many other workers[14,18] have used this model to describe the properties of carbon and graphite fibers. We have used the assumption of uniform stress for all of our calculations. This assumption should be fairly good whenever the crystallites are fairly well oriented. However, it will break down for the crystallites which are poorly oriented. As already noted, the dependence of any of the quantities discussed here on orientation is most sensitive to the tails of the distribution (i.e., the most misoriented crystallites), exactly the region where the uniform stress assumption is least valid. There are numerical techniques now available which enable one to calculate the properties of composite materials which are not in the limits of uniform stress or uniform strain.[20] The use of carefully determined orientation distribution functions along with those techniques may allow us to assess the importance of the highly misoriented crystallites in determining the properties of the fibers.

8. Summary and Conclusions

The mechanical properties of fibers were modelled from the known elastic properties of graphite using a uniform stress approximation. The shear compliance depends critically on the disorder in graphite, and thus was estimated from the Young's modulus and measured crystallite orientation functions. The effective

shear modulus for the crystallites making up these fibers is between 12 and 66E-12/Pa; much less than that found in single crystal. We have also calculated the Poisson ratio and c-axis compression. To date, we know of no direct determination of the Poisson ratio of carbon and graphite fibers.

The piezoresistance was modelled simply as the sum of the geometric changes (determined from the estimates of Poisson's ratio), and the change in carrier density due to the change in interplanar spacing. The model readily explained why the piezoresistance is negative only in fibers which show three dimensional order in their x-ray patterns. All the data fell reasonably well between the limits found by neglecting c-axis strain (as one might expect for turbostratic materials) and including it along with the known dependence of the electron density in graphite. The values obtained for the piezoresistance provide some indications for the best choice of graphite elastic constants and the degree of three-dimensional order, but considerably more work is needed to make these estimates quantitative.

V. PROPERTIES OF INTERCALATED FIBERS

In this section, our work on intercalated fibers is described; with particular emphasis on numerous unpublished results for AsF_5 intercalation compounds. Some preliminary results on the intercaltion of metal-chlorides will be described at the end of the section.

Although intercalation compounds of graphite have been known for many years (for a recent review, see reference 21), interest in them was renewed when it was reported that AsF_5 intercalation compounds had conductivities higher than copper.[22] Although it is now generally accepted that the maximum observed conductivity for AsF_5-graphite compounds is about 0.6 times that of copper, this is still the best conducting intercalation compound presently

known. The high conductivity is due to the large increase in charge carriers caused by the reaction of AsF_5 with graphite along with absence of significant lattice distortion which would reduce the mobility of carriers in the basal planes. Attempts to increase the carrier density beyond that obtained with AsF_5 has generally resulted in a significant reduction in mobility.[23,24] For example, the addition of F_2 to AsF_5 (or other metal-flouride compounds) causes the conductivity to decrease dramatically at high concentrations.[23] We have observed similar behavior in fibers, whereby the intercalation of a metal-fluoride plus F_2 causes the conductivity to go through a maximum before intercalation is complete.[25]

The high conductivity of AsF_5 intercalation compounds would be technologically useful if such compounds could be made in a stable fiber form. Although many graphite fibers are easily intercalated with AsF_5, the conductivity achieved is much lower than that obtained using highly oriented pyrolytic graphite (HOPG). This is because of the importance of defect scattering in fibers, as already discussed. Thus, if the charge transfer is the same as in HOPG, the conductivity of an intercalated fiber will be significantly less than similarly intercalated HOPG. However, it is not completely obvious that the charge transfer will be the same in fibers and HOPG. The small crystallite size and high concentration of defects and disordered carbon could, in principle, affect the chemistry of intercalation. We therefore attempted to determine the importance of fiber microstructure on intercalation of AsF_5 by examining low concentration compounds made from both fibers and HOPG.

Samples were prepared by allowing a predetermined pressure drop from a measured volume of AsF_5, and then sealing the pyrex sample chamber. The actual weight uptake was then determined by weighing the sample along with the pyrex tubing. Since our primary means of study was x-ray absorbtion, samples were designed

to be between 0.3 and 1 absorption lengths for x-rays near the As K edge. This corresponded to fiber samples 1-2 mm thick with a concentration of AsF_5 in the range of 1-10%. Such low concentration samples could not be studied with x-ray diffraction, since the small concentration of AsF_5 did not change the diffraction pattern at all. At slightly higher concentration, high stage material could be observed. When the concentration was 18.5% by weight, stage 9 AsF_5 intercalated graphite could be seen. All diffraction experiments used Mo K radiation so that the sealed pyrex ampules could easily be penetrated with the beam.

When there is no evidence for intercalation, one might have thought that all the AsF_5 had been adsorbed at defects and in the microporosity of the fibers. X-ray absorption clearly showed that this was not the case. First of all, the absorption edge of the AsF_5 was not present, but edges similar to those observed for AsF_6 and AsF_3 were clearly observed. In addition, the amounts of the two species were found to be in a ratio of 2:1, as expected if the reaction were:

$$3AsF_5 \longrightarrow 2AsF_6^- + AsF_3 + 2e^+ \qquad \text{(Ref 10)}$$

Secondly, the polarization of the x-rays could be used to determine that the AsF_3 was oriented in the fibers. The plane formed by the fluorine is parallel to the graphite basal planes.

As shown in Appendix IV, the major difference between our low concentration fiber samples and similarly prepared HOPG samples was that no free AsF_5 could be observed in the fibers. In the HOPG, about 45% of the As was present as AsF_5. This was in agreement with many other estimates of charge transfer in high concentration AsF_5[26], although in clear disagreement with the results of Bartlett et al[10] using x-ray absorption. Although our sample had only 7.5% AsF_5 by weight, it is possible that it was composed of small low stage (i.e., high concentration) regions and pure graphite. In that case, the AsF_5 concentration would be

that expected of a high concentration sample. However, it is suprising that any unreacted AsF_5 would not find the pure graphite and then react further.

The orientation of the As^{+3} species in the fibers is much higher than expected. As shown in Appendix IV, if one assumes perfect orientation and 100% polarization of the x-rays, then one can conclude that the AsF_3 molecule (if that is the As^{+3} species) must be flattened a little in order to explain the polarization dependence of the absoption. All the expected errors and experimental uncertainties would tend to lower the polarization dependence and thus increase the amount by which the AsF_3 is distorted. In addition, when one sample was cryopumped, the orientation dependent part of the signal was significantly reduced. If the orientation effect is coming from only part of the As^{+3} species, that species cannot be AsF_3. The other explanation is that the orientation of the AsF_3 in the graphite is a sensitive function of the equilibrium partial pressure over the sample. Experiments on a larger set of samples, as well as on HOPG are needed to clarify this situation.

Studies of both the electrical and mechanical properties of AsF_5 intercalated fibers were hindered by the lack of stability of these materials. Early efforts to encapsulate samples in a moisture barrier polyurethane (sold as MACAP by Capsulated Systems Inc., Dayton, Ohio) looked promising. Stage 2 AsF_5 intercalated yarns showed no change in x-ray diffraction for six months after being coated with MACAP. A technique for coating single filaments with MACAP without removing them from the vacuum system in which the intercalation was carried out was then developed. The resistance of the intercalated material was stable when extreme care was taken to dry the MACAP and its trichloroethane solvent. However, upon removal of the coated filament from the vacuum system, the resistance increased by at least a factor of

two within an hour. This is probably due to the finite permeability of all polymers to moisture.

After attempts to coat the intercalated sample with a moisture barrier were abandoned, we developed a technique to transfer samples to our helium refrigerator in a vacuum atmosphere glove box. Although the moisture content of the box was kept below 0.5 parts per million, the resistance of the sample always increased by at least a factor of two during the transfer. These difficulties with handling AsF_5-treated fibers for electrical measurements were not expected, based on our experience in preparing samples for x-ray diffraction. Generally, there was no change in x-ray diffraction pattern when samples were prepared by: transferring to a sealed ampule in a glove box; sealing a sealed ampule right off the vacuum system; or coating intercalated samples with polyurethane or epoxy. It is clear that the electrical properties are sensitive to small chemical changes which do not affect the overall structure. Changes in the properties of AsF_5-intercalated HOPG stored in a glove box for many months have been reported by Markowitz.[27] The stability problem is even more serious for fiber compounds because of the small diameter (8-15 micrometers depending upon the degree of intercalation) and large surface to volume ratio for fibers.

In spite of these stability problems, some preliminary mechanical tests were done on stage 2 AsF_5-intercalated ex-PAN yarns which were coated with MACAP and epoxy. As already mentioned, these samples had stable x-ray diffraction patterns. The modulus decreased an average of 15% from similarly prepared yarns which were not intercalated. This decrease was calculated without correcting for the increased diameter of the fibers, since it is expected that only the carbon planes will be load bearing. One can therefore conclude that intercalation does not significantly reduce the Young's modulus of the carbon planes in a high

modulus graphite fiber. This is similar to the results of Oshima and Woolam[28] on $CuCl_2$-intercalated ex-pitch fibers.

We also made well staged metal chloride intercalation compounds using ex-PAN fibers. Stage 2 $FeCl_3$ as well as stage 3 $MnCl_2$-intercalated fibers were synthesized using standard techniques. The resistivity of the $MnCl_2$ intercalated fiber was about 500 micro-ohm-cm, significantly higher than the 300 micro-ohm-cm of the neat ex-PAN fiber. The increase in resistivity of a metal-chloride intercalation compound is very unusual and deserves further study. The temperature coefficient of the resistivity was found to be positive near room temperature, indicating that the fiber was indeed intercalated. $CuCl_2$-intercalated ex-pitch fibers were also synthesized, and the electrical conductivites observed were in good agreement with those obtained by Oshima et al.[1]

VI. CONCLUSIONS AND SUGGESTED FUTURE WORK

There are many interesting questions which deserve additional study. As discussed in the previous section, the As-F species which form in low concentration samples is still unknown. The large changes in electrical properties in high concentration AsF_5 compounds without any observable structural change is also not understood. There are also many other interesting intercalation compounds (such as $MnCl_2$) whose electrical properties are essentially unknown.

In addition to these questions which are directly related to intercalation compounds, our understanding of the structure/property relationships of the neat carbon and graphite fibers is also incomplete. I believe this will be the most fruitful area in which to work, since the neat fibers are already of technological importance, and since an understanding of the properties of

intercalated fibers may depend critically on our understanding of the precurser graphite.

Our efforts at modelling both the electrical and electromechanical properties of neat carbon and graphite fibers has already improved our understanding of these materials. These have relied on careful x-ray diffraction characterizations of three dimensional order and orientation. It is important that the diffraction work be continued to help our understanding of the nature of the correlations which occur even in turbostratic material. Crystallite size measurements as a function of orientation in the fiber will also improve our picture of the microstructure of these materials. The combination of piezoresistance with hydrostatic pressure measurements will provide an important test of our models. With the increase in information provided by these experiments, it will be possible to test more sophisticated elastic and electronic models which will enable more quantitative predictions to be made.

We have been successful in modelling high modulus fibers primarily because their properties are dominated by the properties of the graphite crystallites of which they are composed. This is not the case for the more disordered carbon fibers, and efforts should continue to understand the nature and importance of the disordered carbon in these materials. Futhermore, fundamental studies should be extended to include even lower heat treated pyrocarbons. These materials are becoming increasingly important technologically. In addition, an understanding of the materials which are made before carbonization is complete will lead to a better understanding of the process by which high strength carbon fibers are made.

REFERENCES

1 H. Oshima, J. A. Woolam, and A. Yavrovian, J. Appl. Phys, 53, 9220 (1982)

2 T. S. Dziemianowicz and W. C. Forsman, Synthetic Metals, 8, 297 (1983).

3 M. Endo, T. C. Chiev, G. Timp, and M. S. Dresselhaus, Synthetic Metals, 8, 251 (1983).

4 A. A. Bright, Phys. Rev. B, 20, 5142 (1979).

5 C. N. Owston, J. Phys. D, 3, 1615 (1970).

6 K. Komaki, PhD Dissertation, University of Washington, May, 1980 and D. B. Fishback, K. Komgki, and S. Srinivasagopalan, FINAL TECHNICAL REPORT on US Army Research Office grant DAAG29-76-G-0169, July 1980.

7 I. L. Kalnin and H. A. Goldberg, Extended Abstracts of the 15th Biennial Conference on Carbon, 367 (1981).

8 P. Kwizera, A. Erbil, and M. S. Dresselhaus, Carbon, 19, 144 (1981).

9 A. S. Fialkov et al., Izvestiya Akademii Nauk SSSR, Neorgnicheskie Materialy, 14, 889 (1978).

10 N. Bartlett, R. N. Bianconi, B. W. McQuillan, A. S. Robertson, and A. C. Thompson, J. Chem. Soc., Chem. Comm., 200 (1978).

11 G. J. Curtis, J. M. Milne, and W. N. Reynolds, Nature, 220, 1024 (1968).

12 B. T. Kelly, Physics of Graphite, Applied Science Pub. (1981).

13 D. B. Fishback and S. Srinivasagopalan, PROCEEDINGS OF THE FIFTH LONDON INTERNATIONAL CARBON AND GRAPHITE CONFERENCE, 389 (1978); and, S. Srinivasagopalan, PhD Thesis, University of Washington (1979).

14 W. N. Reynolds and R. Moreton, Phil. Trans. of the Royal Society of London, A, 294, 451 (1980).

15 D. B. Fischbach, 37th PACIFIC COAST REGIONAL MEETING OF THE AMERICAN CERAMICS SOCIETY, San Francisco, CA 1984).

16 I. L. Spain, Private Communication.

17 W. Ruland, Applied Polymer Symposia No. 9, 293 (1969).

18 C. P. Beetz, Jr., 15th BIENNIAL CONFERENCE ON CARBON EXTENDED ABSTRACTS, 302 (1981).

19 R. J. Price, Phil. Mag., 12, 561 (1965).

20 C. T. D. Wu and R. L. McCullough, Developments in Composite Materials-1, G. S. Holister Ed., Applied Science Publishers, 119 (1977).

21 M. S. Dresselhaus and G. Dresselhaus, Advances in Physics, 30, 139 (1981).

22 G. M. T. Foley, C. Zeller, E. R. Falardeau, and F. L. Vogel, Solid St. Communications, 24, 371 (1977).

23 T. E. Thompson, E. M. McCarron, and N. Bartlett, Synthetic Metals, 3, 255 (1981).

24 A. Metrot and J. E. Fischer, Synthetic Metals, 3, 201 (1981).

25 I. L. Kalnin and H. A. Goldberg, Synthetic Metals, 3, 159 (1981).

26 M. Saint Jean, N. H. Hav, C. Rigaux, and G. Furdin, Solid State Communications, 46, 55 (1983).

27 R. S. Markiewicz, Solid State Communications, 44, 791 (1982).

28 H. Oshima and J. A. Woolam, Synthetic Metals, 5, 113 (1983).

PUBLICATIONS

1. S. Heald, H. A. Goldberg, and I. L. Kalnin, "Application of EXANES to the Study of AsF_5 Graphite Intercalation Comvounds," in Springer Ser. Chem. Phys., Vol. 27, p. 141, (1983).

2. I. L. Spain, K. J. Volin, H. A. Goldberg, and I. L. Kalnin, "Unusual Electrical Resistivity Behavior of Low Modulus Carbon Fibers," Solid St. Communication, 45, 817 (1983).

3. I. L. Spain, K. J. Volin, H. A. Goldberg, and I. L. Kalnin, "Electronic Properties of PAN-Based Carbon Fibers I. Experiment and Comparison with Properties of Bulk Carbons," Physics and Chemistry of Solids, 44, p. 839, (1983).

4. H. A. Goldberg, I. L. Kalnin, I. L. Spain, and K. J. Volin, "Unusual Resistivity Maximum in Low Modulus Carbon Fibers," Extended Abstracts of the 16th Biennial Conf. on Carbon, p. 281, (1983).

5. J. Stamatoff, H. A. Goldberg, and I. L. Kalnin, "X-ray Diffraction Studies of Structural Dimensionality in Carbon Fibers," Proceedings of the Mtl. Res. Soc. Symposium on Intercalated Graphite, (1982).

6. I. L. Kalnin, H. A. Goldberg, J. B. Stamatoff, and I. L. Spain, "Structure and Intercalation of Carbon Graphite Fibers," Extended Abstracts of the 16th Biennial Conf. on Carbon, p. 274, (1983).

APPENDIX I

J. Phys. Chem. Solids Vol. 44, No. 8, pp. 839–849, 1983
Printed in Great Britain

0022-3697/83 $3.00 + .00
Pergamon Press Ltd

ELECTRONIC PROPERTIES OF PAN-BASED CARBON FIBERS—I

EXPERIMENT AND COMPARISON WITH PROPERTIES OF BULK CARBONS

I. L. SPAIN† and K. J. VOLIN
Department of Physics, Colorado State University, Fort Collins, CO 80523, U.S.A.

and

H. A. GOLDBERG‡ and I. KALNIN
Celanese Research Company, Summit, NJ 07901, U.S.A.

(*Received* 30 *August*; *accepted* 15 *December* 1982)

Abstract—Measurements of the resistivity of PAN-based fibers are reported for temperatures between 1.5 and 300 K. Particular care was taken to avoid sample heating problems during measurements. Fibers were heat-treated between ~1300°C to above 3000°C, corresponding to a wide range of elastic moduli (~35–112 Msi, 240–770 GPa). A particularly surprising result was the observation of a resistivity maximum for low modulus (35 Msi ~240 GPa) fiber below 50 K. Results are compared to those reported on bulk heat treated carbons and pyrocarbons. A qualitative discussion of the results is also given in terms of recent models of the electronic energy levels of carbon ribbons and turbostratic carbons.

1. INTRODUCTION

Carbon fibers represent one of a class of carbons which include heat-treated organic precursors, pyrolytic carbons, glassy carbons, evaporated carbons, carbon blacks, etc. The properties of these materials depend sensitively on the microstructure and local bonding arrangement of the carbon atoms (for a review, see Ref.[1]).

Although carbon fibers were first used commercially by Edison before 1880, these materials were isotropic and of low strength. High strength fibers were prepared in 1964 by groups in Great Britain (see Ref.[2]) based on polyacrylonitrile (PAN) and in the U.S. (see Ref.[3]) using a rayon precursor. More recently, pitch-precursor fibers have been prepared with improved structural properties[4]. Even further improvements have been reported using vapor deposition techniques[5].

In this paper we will be concerned with fibers based on PAN precursors which are used commercially. These fibers are prepared from commercial PAN textile by a cross-linking heat-treatment in air at ~220°C, followed by carbonization at between 1000 and 1300°C or partial graphitization between 2200–3000°C, in an inert atmosphere. The highest heat-treatment temperature (HTT) is an important processing parameter, which is often used to label the fiber properties. It is recognized that carbonization and graphitization are kinetic processes and that residence time at HTT is an important parameter[6]. It will be assumed that residence time is fixed. It is stressed that HTT is only a convenient label to distinguish one fiber from another, and that it should be used with caution.

†Work supported by a grant from Celanese Research Co.
‡Work supported by U.S. Army Research Office

Several PAN fibers were examined in this work. One of them was heat-treated at a relatively low temperature (~1300°C) and has a relatively low value of Young's modulus (~35 Msi, ~240 GPa). At this temperature, the fibers are impure carbons with typically a few percent of nitrogen and of the order of tenths of percent of various inorganic impurities. Other fibers tested have higher moduli (up to 114 Msi ~770 GPa) from heat treatment to greater than 3000°C. These fibers are less impure and have more highly developed structure. Although fibers prepared from different precursor materials (e.g. rayon, PAN, pitch...) would need to be treated differently to achieve this modulus, the electrical resistivity at room temperature has been found to correlate well with Young's modulus[7].

Certain gross structural features are common to all carbon and graphite fibers (see Fig. 1). The extended aromatic networks lie parallel to one another and roughly parallel to the fiber axis. In a plane parallel to the axis, these planar networks undulate with mean misorientation angle which may be in the region ~8–30°. In the direction of the fiber axis, the mean distance along relatively straight portions of the networks is ~100 Å (10 nm) but the networks must be connected over much longer distances than this. In the plane perpendicular to the fiber axis, the networks are probably less extensive and more disordered with respect to angular misalignment. There are still some uncertainties concerning the details of the microstructure, but Fig. 1 is probably representative of current thinking.

There are differences between the structures of fibers prepared from different precursors, related to the manner in which the networks are organized in the plane perpendicular to the axis[8]. For instance, the hexagon

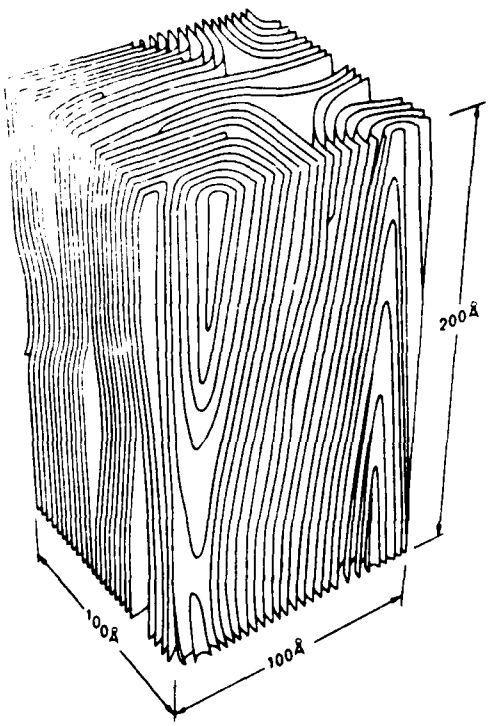

Fig. 1. Sketch of the structure of a high strength carbon fiber. The fiber axis is vertical. (Figure adapted from Wicks[9].)

planes often lie roughly in a circumferential fashion about the fiber axis in ex-rayon fibers, radially or random in ex-pitch fibers, and in an intermediate, more disordered fashion in ex-PAN fibers. It is noteworthy that ex-pitch fibers pass through a liquid mesophase during the heat-treatment process, so that the aromatic networks organize and order more readily under the same heat-treatment conditions as other fibers[4].

Certain physical properties of bulk heat-treated carbons, pyrocarbons and carbon fibers appear to vary in a similar way as heat-treatment temperature increases[1, 2, 10, 11]. Figure 2 sketches the variation of some structural and electronic properties, as proposed by Mrozowski[12] for bulk carbons, with some data added by us for fibers and pyrocarbons. As seen in Fig. 2, the resistivity (ρ) of bulk carbons falls as HTT increases, while the "crystallite size" (L_a) increases. The Hall constant (R_H) changes sign at HTT ~1700°C and 2400°C. The magnetoresistance ($\Delta\rho/\rho_0$) is small and takes negative values for a range of HTTs. Although there are some differences between bulk carbons and fibers, the trends are similar. Other analogies will be drawn later in the paper.

Data will be presented on the resistivity of ex-PAN fibers and the results will then be discussed by analogy with other carbons and using recent models of the electronic structure.

2. EXPERIMENTAL TECHNIQUES

Fibers were mounted on ceramic plates by attaching them to four conducting strips using conducting epoxy. Constant current (~10 μA) was passed through the fiber via the end contacts, and the potential developed across the fiber was measured using the two inner contacts approx. 10 mm apart. Typical sample resistances were ~500–5000 Ω. Sample resistances were measured by taking the average of readings for both current directions. Current was measured similarly from the potential developed across a calibrated resistor. Measurements were made between ~1.5 and 4 K with direct immersion in liquid helium. Above this temperature, the sample was immersed in gaseous helium at 1 atm pressure.

It was found that small, irreproducible, changes were recorded in the measured values of resistance upon temperature cycling. These effects were believed due to small changes in contacts or in the bulk of the samples. It is stressed that carbons are inhomogeneous, anisotropic ceramics so that changes in temperature produce stresses and strains which may lead to crack formation and propagation. Extensive cycling tests were carried out. It was found that changes of resistance of magnitude less than one part in 10^3 occurred in an unpredictable way upon cycling, but that the resistance remained constant to within experimental error (~1 in 10^5) over long periods of time at fixed temperature, while the magnetoresistance ($\Delta\rho/\rho_0$) also remained constant after cycling, even if the base resistivity shifted slightly. Similar effects were observed also on bulk carbons[15]. Consideration of sample heating effects is made in Appendix A.

The resistance of the fiber could be determined to an accuracy of ±0.01%. However, the length of the fiber could only be determined to ±1%. The cross-section of low modulus fibers was found to be nearly circular and the area could be determined to ±7%. However, the cross-section of the higher modulus fibers was found to be irregular (dog bone) and the area could only be determined to an estimated accuracy of ±20%.

3. RESULTS

(a) *Higher modulus fibers* (350–770 GPa; 50–112 Msi)

Resistivity curves for all fibers are included in Fig. 3, where comparison is made with similar data for bulk carbons. In all cases, the resistivity increases as temperature falls (negative coefficient of resistance), with the exception of the low-temperature behavior of the lowest modulus fiber.

The temperature dependence of the resistivity is seen more clearly in Fig. 4 where the function $F(T) \equiv \rho(0)/\rho(T) \equiv \sigma(T)/\sigma(0)$ (σ = conductivity) is plotted. Also, resistivity and other data for the fibers are given in Table 1. Trends are clear:

(1) Resistivity falls with increasing HTT. Compared to heat-treated bulk carbons, the resistivity is lower for the same value of HTT, except above ~2700°C (Fig. 2), while the curve for pyrocarbons is even lower than for fibers. This is presumably related to the orientation of ribbons in the fibers along the fiber axis. Pyrocarbons are also oriented, and resistivity is correspondingly lower than bulk mesophase carbons.

(2) Relative changes of resistance with temperature

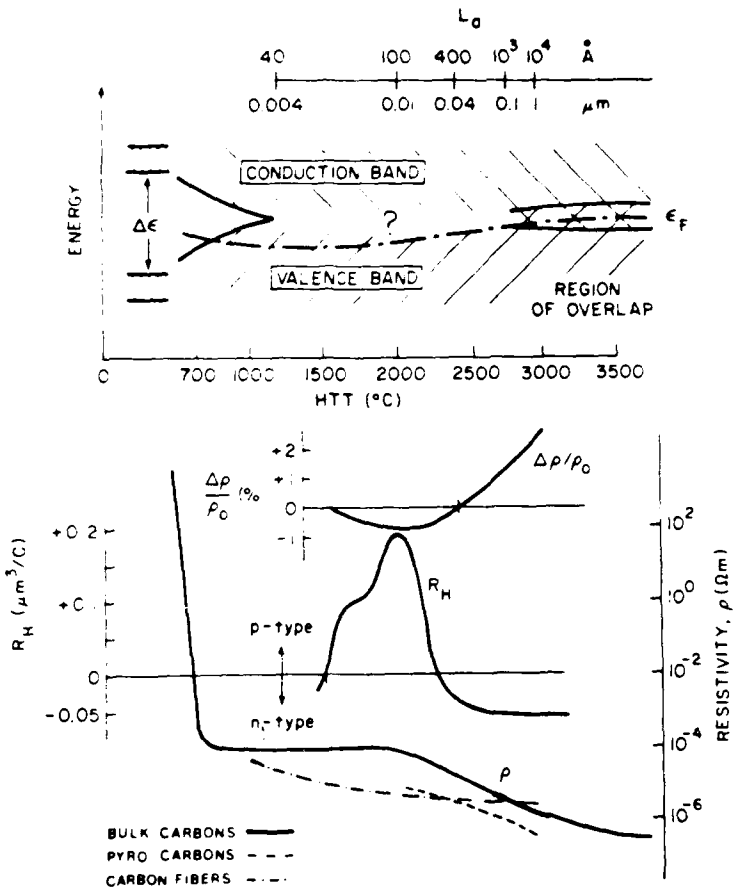

Fig. 2. Sketch of the variation of electrical resistivity and magneto-resistance of heat-treated bulk carbons, pyrocarbons and fibers, as a function of HTT. Crystallite size for bulk heat-treated carbons is indicated. Also included is a sketch of a simple band model proposed by Mrozowski[12] to qualitatively explain the results. Data from Refs [4, 11] (carbon fibers); [13] (bulk carbons); [14] (pyro-carbons).

Table 1. Summary of fiber properties

Sample	HTT (°C)	d(Å)	Density (g/cm^3)	ρ(300K) μΩm	Young's Modulus GPa	Psi
A	3000	3.43	2.12	3.2	770	112
B	3000	-	2.08	3.7	730	106
C	2500	3.43	2.01	5.5	600	87
D	2500	3.43	1.96	6.5	500	72
E	2000	3.43	1.85	10.5	350	51
F	1500	-	-	15	240	35

[illegible] and Thornel 300.

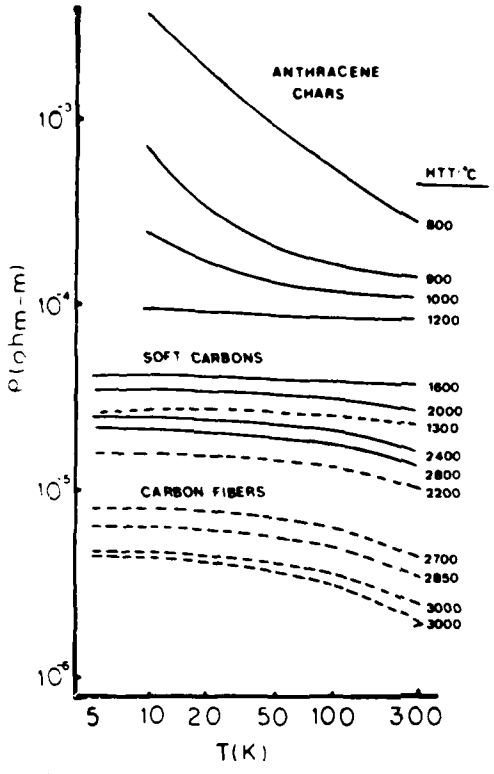

Fig. 3. The variation with temperature of the resistivity of bulk carbons (——) and fibers (– – – –). Data from Refs.[18] (anthracene chars);[15] (soft carbons); and present work (carbon fibers).

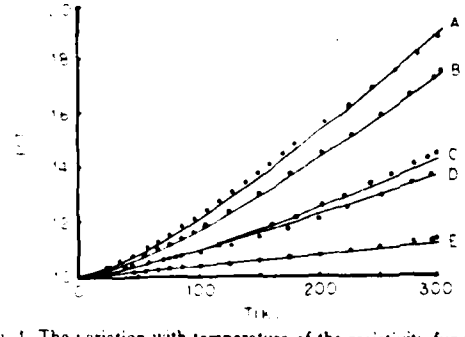

Fig. 4. The variation with temperature of the resistivity function $\rho(0)/\rho(T)-1$ for several fibers. Identification of fiber types is given in Table 1. Theoretical points are discussed in Section 4(b).

are greater for higher modulus fibers heat-treated to higher temperature.

These trends are similar to those observed by other workers[4, 10, 11].

(b) *Low modulus fibers* (240 GPa; 35 Msi)

The most unusual result of the present measurements is the occurrence of a maximum in the resistivity at ~25 K for the Thornel 300 fiber and ~35 K for the Celion 3000 and Magnamite fibers, plotted in greater detail in Fig. 5. The resistance maximum for the Thornel 300 fiber is sharper than that for the Celion 3000 and Magnamite fibers. However, the overall form of $\rho(T)$ for the three types is similar. The ratio of $\rho_{max}/\rho_{4.2\,K}$ equals

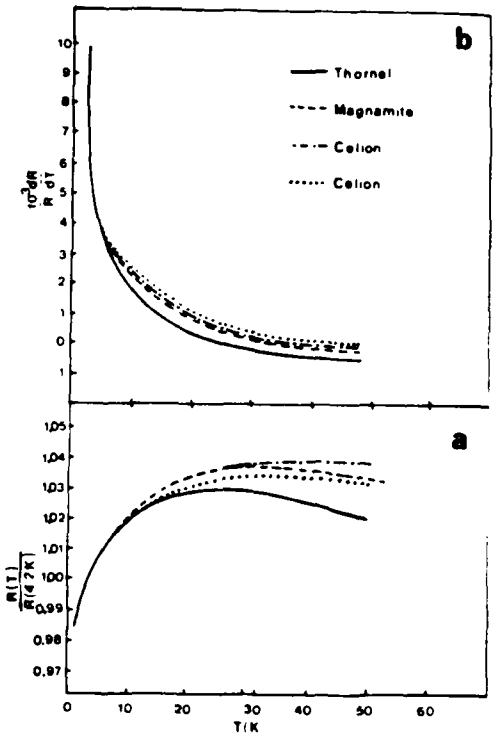

Fig. 5. (a) The variation with temperature of the reduced resistivity of low modulus carbon fibers below 50K. (b) The temperature dependence $1/R\ dR/dT$ below 50 K.

1.027, 1.034 and 1.036, respectively, for the Thornel, Celion and Magnamite fibers, for comparison of these three fiber types.

Measurements were taken down to 1.5 K by pumping on liquid helium. At the lowest temperature, the positive slope, dR/dT, was not diminished for any of the fibers, as shown in Fig. 5.

4. DISCUSSION

(a) *General trends and comparisons with other carbons*

Much of our understanding of the properties of carbons comes from heat-treatment of bulk aromatic hydrocarbons. Since the electrical properties of commercial fibers evolve in a similar way to these bulk carbons, as structural perfection increases, a brief outline of the properties of bulk carbons will be given first.

A model for the variation of measured properties and evolution of "crystallite" size and electronic structure of bulk carbons is given in Fig. 2, due to Mrozowski[12]. There are three major types of electronic behavior which result when bulk graphitizing carbons are heat-treated.

(1) Non-conducting, impure carbons result from HTT ≤800°C. The material can be regarded as a collection of aromatic molecules consisting of a few rings. Coulson *et al.*[16] showed for several benzene-derivative systems that the gap separating bonding and antibonding states closes as the number of the aromatic rings in the molecule increases. Accordingly, the steep drop in the resistivity vs HTT curve can be attributed to the increase in the mean molecular size.

(2) Graphite material results from very high HTTs (e.g. ≥3000°C). In this region, the bulk carbon approximates a graphite with small crystallite size. Graphite is the semimetallic three-dimensional, crystalline form of carbon, in which there is a regular *ABAB* stacking sequence of the layer planes, and in which the valence and conduction bands overlap by ~40 meV[17]. Heat-treated carbons graphitize to different extents after typical heat-treatment times, so that property differences are expected between bulk mesophase carbons and fibers prepared from various precursors.

(3) Turbostratic carbons result from intermediate HTTs (800 ≤ HTT ≤ 3000°C). All of the fibers studied in this paper fall into this category. Properties at the upper end of the HTT range depend sensitively on the type of carbon. *Certain bulk carbons graphitize well below* 3000°C. The conventional picture of a turbostratic carbon emphasizes the random stacking of aromatic networks, as opposed to the regular *ABAB* stacking sequence of crystalline graphite. A subsequent paper will consider the structure of the fibers in greater detail.

At the lower end of this range, the resistivity versus temperature plots indicate a change from "semiconducting" to "metallic". This transition has been investigated in detail by Delhaes and collaborators (see Ref.[18] for a review). They argue that metallic carriers exist in isolated regions well before the onset of bulk metallic conductivity, and that the transition is of the percolative[19] type. In this case, macroscopic conductivity arises when regions of relatively high conductivity link over the dimensions of the sample so that a high conductivity path becomes available.

In the intermediate HTT region (e.g. 900 ≤ HTT ≤ 1800) the resistivity remains roughly constant for bulk carbons, while the Hall coefficient changes from negative below ~1700°C to positive above. The magneto-resistance is very small below ~1500°C but is negative for HTT ≤2300°C. Hall data have not been reported for fibers. However, thermoelectric power measurements have been made on ex-PAN fibers[10] and are compared to similar data on bulk samples[20] which closely follow Hall data (Fig. 6). The two curves follow closely, crossing zero at HTT ~ 1100°C and 1600°C. Above HTT ~ 2300°C, differences are expected between the behavior of ex-PAN fibers and bulk, mesophase carbons, because of the relative ease with which the bulk carbons graphitize.

If the change of sign of the Hall coefficient and thermopower for HTT ~1700°C can be related to the passage of the Fermi level through the region of separation, touching or overlap of the conduction and valence bands, then it would be expected for the density of states and density of free carriers to pass through a minimum. The density of free carriers has been estimated by Arnold and Mrozowski[21, 12] from esr measurements, and their *results are depicted in Fig 7. No minimum* is observed near HTT ~1700°C. Also, the variation of resistivity is smooth through this range of HTT.

(b) *Earlier band models for turbostratic carbons*

Mrozowski[12] indicated that there were no good models for the electronic energy bands in this region, marking it with a question mark (Fig. 2). Boy and Marchand[22] also considered several simple models for the bands and tried to fit values of the para- and diamagnetic susceptibilities and the Hall effect simultaneously, without success.

An example of the difficulties encountered with the use of simple band models can be seen from the work of Bulawa *et al.*[23], who carried out measurements on the variation of Hall coefficient of bulk carbons doped with acceptors and donors. They interpreted their results in terms of a simple two-band model. The band overlap was then inferred from the variation of the Hall coefficient with doping. Surprisingly, it was found that for HTT ≥2400°C the band overlap remained roughly constant. This is the range of HTT where X-ray data indicate that graphitization occurs, so that the band overlap should vary from close to zero for HTT ~2400°C to the value for single crystal graphite (40 meV) at HTT ~3500°C. In the range 2200 < HTT < 2400°C, a 20% decrease in the

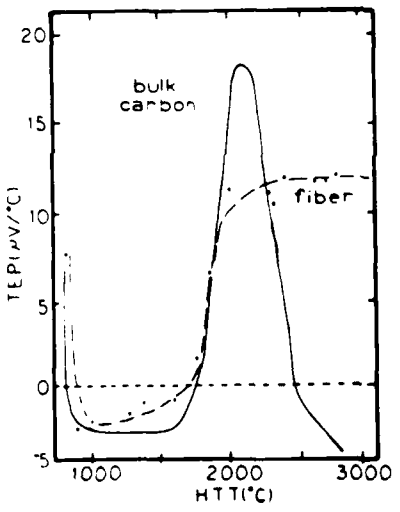

Fig. 6. Comparison of thermoelectric power data for bulk carbons[20] and carbon fibers[10] both as a function of HTT.

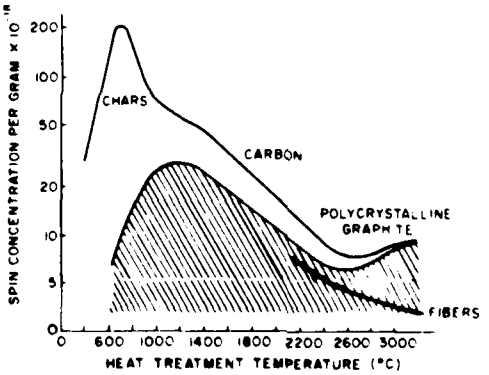

Fig. 7. A sketch of the variation of localized carrier concentration (upper curve) and the density of free carriers (hatched curve) for heat-treated carbons, as obtained from electron spin resonance[12]. Data for fibers using the simple two-band model are also included.

band overlap was inferred, then an *increase* in the overlap for HTT $\leq$2200°C.

A similar trend is found if the conductivity-temperature curves are fitted for the present fibers. Klein[24] found that a simple two-band model (STBM) could fit the carrier density for a number of pyrocarbons over a measurement temperature range 4–1500 K. The model is illustrated in Fig. 8. Electron and hole bands are both assumed to be quadratic ($\epsilon \alpha k^2$) with band overlap ϵ_0. By making the simplifying assumption that electron and hole mobilities are equal (μ) and independent of temperature, the ratio of conductivity at temperature T to that at $T = 0$K can be expressed as

$$F(T) \equiv \frac{\sigma(T)}{\sigma(0)} = \frac{kT}{\epsilon_0 - \epsilon_f}\{\ln[1 + e^{\epsilon_f/kT}] + \ln[1 + e^{(\epsilon_0 - \epsilon_f)/kT}]\} \text{ for } \epsilon_f < 0,$$

$$= \frac{kT}{\epsilon_0}\{\ln[1 + e^{\epsilon_f/kT}] + \ln[1 + e^{(\epsilon_0 - \epsilon_f)/kT}]\} \text{ for } \epsilon_f > 0.$$

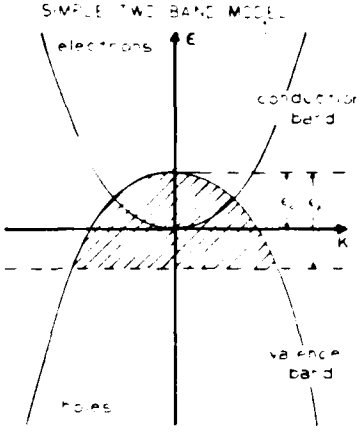

Fig. 8. Energy wave-vector relationship for the simple two-band model used in the text. ϵ_0 is the band overlap.

A typical fit to the data is illustrated in Fig. 9 for fiber *B*. Data obtained for fibers *A* through *E* are given in Table 2, based on a model in which ϵ_f was held constant with temperature.

Two important qualitative features emerge from these data: (1) The band overlap ϵ_0 increases with decreasing modulus, as found by Bulawa *et al.*[23] from Hall studies. (2) The Fermi level lies near, but below, the bottom of the conduction band.

In order to proceed further, additional details need to be specified for the model. The following procedure was adopted. Firstly, it was assumed that the mean free path, λ, for fiber *E*(HTT = 2200°C) was 40 Å. Then the model was used to calculate the effective mass ratio, $m^* m_e = 0.012\, m_0$, assuming equal masses for the conduction and valence bands (Table 2). Then, using this effective mass value, the mean free path was calculated for the other fibers *A* through *D*. Also, the Fermi speed, V_F, and density of carriers, *P*, were calculated. The Fermi speed compares with the energy-independent value for the Wallace model[26] of 1.0×10^6 m sec ($V_F = \sqrt{3} a \gamma_0 / 2\hbar$, where a is the lattice constant (2.46 Å) and γ_0 the in-plane overlap integral (3.0 eV) which is obtained for the ideal graphite sheet.) Carrier densities are compared with those obtained by Mrozowski[12] for bulk carbons from esr data in Fig. 7. The values obtained here are below his estimates.

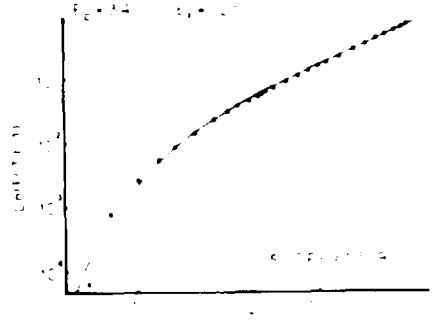

Fig. 9. Representative data and fit for the temperature dependence of resistivity (fiber B).

Table 2. Parameters obtained from simple two-band model

Sample	HTT	ϵ_0(eV)	ϵ_F^*†(eV)	$P^*(10^{24}/m^3)$	$P^*(10^{18}/gm)$	$V_F^*(10^6 m/s)$	λ^*(Å)
A	>3000	.025	.027	2.7	1.3	0.87	300
B	3000	.029	.031	3.2	1.5	0.94	230
C	2850	.043	.046	4.7	2.3	1.14	130
D	2700	.052	.053	5.4	2.8	1.23	100
E	2200	.134	.136	13.6	7.4	1.95	40

†From top of valence band.

*Assuming $m^* \cdot m_0 = 0.012$.

P = hole density.

It is emphasized that this model is extremely artificial. Parameters for the band model have been forced to fit the unusual temperature dependence of the resistivity using a temperature-independent mobility. A single band model would not be capable of fitting the data without introducing defect levels with temperature-dependent occupancy. Although more reasonable models could be constructed, none would be capable of explaining the unusual combination of resistivity, Hall and esr properties for HTT near 1700°C.

However, an important point needs to be stressed. The overlap of the two bands in a simple two-band model needs to *increase* with decreasing HTT. Although the values of ϵ_0 shown in Table 1 depend on the simple band model used, the general trends are independent of this model. The rate at which resistance changes with temperature depends on kT/ϵ_0, where ϵ_0 is the characteristic overlap energy. We feel that this qualitative feature is independent of the details of the two-band model adopted. This result is at variance with theoretical models of the energy bands to be discussed in the next section.

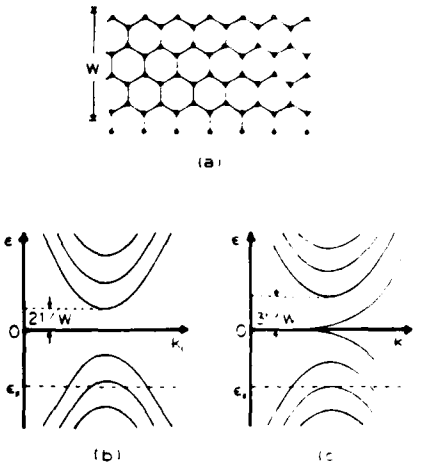

Fig. 10. (a) Sketch of the ribbon used by Chausse and Hoarau[30]. (b) One-dimensional energy levels for the carbon ribbon with lower edge atoms (model 1). (c) Without lower edge atoms (model 2).

(c) *Theoretical models of the energy bands*

Recently, theoretical models have been developed for the band structure of carbons. Firstly, McClure and Ruvalds[25] showed that the band structure of turbostratic carbon (graphite sheets stacked in a random manner) was identical to that of a single sheet[26]. The Landau levels for these two-dimensional sheets are unusual[27]. Bright[28, 29] developed a modified model of this type to explain semi-quantitatively the magnetoresistance, including negative values. It was necessary to allow the energy levels to be broadened due to the short mean free path of the carriers resulting from collisions with defects. In addition, acceptor levels and localized states at the band touching region were postulated.

Chausse and Hoarau[30] have considered the electronic structure of sheets of carbon atoms in the form of narrow ribbons. Two models were considered. The ribbon for model 1 has an odd number of rows (one edge smooth, the other with edge atoms, Fig. 10), while an even number (two smooth edges) characterizes model 2. In both cases, the electron states consist of a set of one-dimensional dispersion relationships, as sketched in Figs. 10(b) and 10(c), with wave-vector parallel to the ribbon length. In model 1, there are localized states at $\epsilon = 0$, so that a semiconductor with gap 2Δ results. The localized states are joined to dispersive states in model 2, so that a zero-gap semiconductor results.

Separation between energy states is indicated in Figs. 10(b) and 10(c), where W is the width of the ribbon (Fig. 10a). Since ribbon widths ~100–500 Å are to be expected in fibers, energy separations ~0.3–0.06 eV are expected. Calculations are much simpler for model 2. Values for effective masses in the range ~0.01–0.1 m_0 are expected for the lowest branch. These models have been developed by Hoarau and Volphilac[31] to yield the magnetic susceptibility, while corresponding data for fibers have been fitted by McClure *et al.*[32]. We emphasize that these models predict either zero or finite energy gap, rather than overlap, in contrast to phenomenological models needed to fit the data.

Ribbon widths are difficult to estimate from X-ray or electron microscope examinations, since the ribbons are probably folded (see Fig. 1). Estimates from the above fits to the susceptibility[32] are several times larger than those from conventional structural techniques, probably because a ribbon cannot be "seen" in entirety (phase contrast effects). As HTT decreases, W decreases so that the effective mass increases and energy separation between branches increases. These features cannot alone explain the temperature dependence of the resistivity, nor can either of the models 1 and 2 account for the resistivity, Hall and esr results near 1700°C HTT.

(d) *The role of sample inhomogeneity*

In the preceding sections, it has been pointed out that band models can be used to fit a particular piece of experimental information, but that an overall explanation of observed phenomena is lacking. In this section, quantitative arguments will be put forward for the role of inhomogeneity to be important in explaining observed phenomena.

Mrozowski *et al.*[33, 34] have discussed briefly the role of a different type of inhomogeneity to that discussed here. In one case[33] the possibility that photo-injected carriers could accumulate on larger molecules, leading to variation of charge distribution, was discussed. In another case[34], the possibility of there being a distribution of donor or acceptor molecules was discussed for doped carbons.

The type of inhomogeneity which will be considered here is of a more intrinsic nature. It arises because of the statistical distribution of aromatic network sizes and shapes (molecular sizes and shapes).

Coulson *et al.*[16] considered the electronic states of large aromatic molecules of different symmetries and edge configurations. They concluded that the energy separating filled and unfilled states decreased with in-

crease in molecular size, and that the density of states of a single sheet of carbon was being approached for molecules with more than about 50 carbon atoms. However, their calculations also showed that the energy between the center of the gap and the vacuum level (intrinsic work function) changed considerably for different molecule configurations.

This implies that a collection of molecules in a solid would need to exchange charge in order to equalize the electrochemical potential. In order for these effects to be important, the scale of the inhomogeneity must be less than the screening length. This is so for turbostratic carbons in which charge exchange is between adjacent aromatic networks of different sizes and edge configurations (i.e. between neighboring hexagonal planes). Undoubtedly, this is also the reason for the precolative nature of the insulator-to-metal transition near HTT ~900°C [18]. Metallic regions in a non-metallic matrix would correspond to molecular configurations with high or low values of work function (for the isolated molecule) which have donated or accepted charge to give a Fermi energy lying in the conduction or valence band.

Although Coulson *et al.*[16] show that changes in size and configuration of molecules can give rise to changes in intrinsic work function, it is also possible that other factors could contribute to inhomogeneous effects. For instance, suppose that the material consists of a set of molecules with the same intrinsic work function, but varying band gaps, then overlap of the anti-bonding levels in one molecule could occur with the bonding levels for another molecule, provided that donor and/or acceptor impurities are present inhomogeneously. We prefer to believe that the inhomogeneity is caused by a statistical variation of molecular size and shape (varying band gap and intrinsic work function) since the variation of properties with HTT follows a closely uniform pattern for carbons prepared from a wide range of precursors, and in different forms (e.g. bulk materials and fibers). Ex-Pan fibers, for example, contain nitrogen impurities, which should act as donors. However, their electrical behavior is similar to that of anthracene chars.

The band model which we envisage for carbon fibers and turbostratic carbons generally would depend in an important way on the inhomogeneity. Each aromatic network (e.g. a simple ribbon of carbon atoms in a fiber) would have a density of states characterized by either zero or positive band gap, as in the Chausse and Hoarau model. In addition, there would be localized states in the gap or region of band touching. Since the work function of each network is different, the aggregate density of states would be similar to that in Fig. 11(a) and 11(b). Depending on the precursor material and HTT, there would be donor or acceptor levels. Acceptors are illustrated in Fig. 11.

With a model of this type, the main features of the results can be explained qualitatively:

(1) $HTT \leq 600$°C. In this range of HTT, the energy gaps between bonding and antibonding levels are sufficiently large, that a net energy gap exists, in spite of variation of intrinsic work function.

(2) $600 \leq HTT \leq 800$°C. In this range, the energy gaps

Fig. 11. Sketch of a possible density of states curve for a disordered, inhomogeneous carbon. The curve is the aggregate for the whole material.

decrease to sufficiently small values that the influence of statistical variations of gap and intrinsic work function become increasingly important. Aromatic networks have net charge in some cases, so that small conducting regions increase with HTT, until the percolation threshold is reached.

(3) $800 \leq HTT \leq 1500$°C. The gaps continue to decrease as the aromatic networks enlarge. The overlap of bonding and antibonding states steadily increases, so that the density of conduction electrons increases (see Fig. 7). Since the maximum carrier density is $\sim 5 \times 10^{-3}$ holes/carbon atom, the overlap of states due to work function variations must be ~0.1 eV.

(4) $-1500 \leq HTT \leq 2300$°C. Increasing aromatic network growth leads to a decrease in energy gaps between states, and the variation of intrinsic work functions, so that the net overlap of "antibonding states" and "bonding states" decreases. At the minimum in the carrier density curves of Fig. 7, the overlap must be reduced to ~0.03 eV (see also Table 2).

(5) $HTT \geq 2300$°C. In this region, bulk mesophase carbons tend to graphitize, while ex-PAN fibers graphitize to a lesser extent. With graphitization, a true band overlap can occur due to the coherent interaction of carbon atoms in neighboring aromatic networks.

Within this model, the position of the Fermi level may be fixed by a number of factors, such as impurities, boundary atoms or configurations at the edge of aromatic networks, vacancies, etc. It is probably impurities which give *n*-type behavior below HTT ~1600°C, but vacancies which give the *p*-type character for HTT ≥ 1600°C. The model explains in a simple way why the Hall coefficient can change from *n*- to *p*-type for HTT ≈ 1600°C, but the density of free electrons varies smoothly (see Fig. 7). The above features of the model also account for the Hall measurements of Bulawa *et al.*[23] on doped carbons, from which they inferred an *increase* in band overlap for HTT ≤2200°C.

An unusual feature of the present model—the simultaneous existence of localized and delocalized states for a given energy value—explains why the conductivity does not fall for HTT ~1600°C, where the Fermi energy lies in the localized states region. The delocalized electrons are associated with the interior, the localized states with the edge regions, of the aromatic networks. Consequently, conduction can occur along the interior of the ribbons in fibers and not be dependent on hopping of carriers in localized states, provided that continuous current paths are available.

This feature of the model can also explain a very recent

result on the high temperature behavior of fiber resistivity. Beetz[35] found evidence for hopping conductivity in high strength carbon fibers above room temperature. This may be interpreted as an additional contribution to the conductivity which arises when the Fermi level is pushed into the region of localized states due to thermal compensation. Additional conduction paths may be opened up, necessitating the hopping of carriers from one ribbon to another. Hopping type conductivity found in glassy carbons[36] may also be explained by this model.

Calculations are being initiated to assess whether the effects of inhomogeneity can account for observations in a quantitative way.

(e) *The anomalous resistivity-temperature curve for low modulus fibers*

The major trends in the electronic properties can be understood qualitatively, as described above. However, the maximum observed in the resistivity of the 240 GPa fibers cannot be understood within this framework. As outlined above, it is anticipated that the fiber would be inhomogeneous.

Anomalies in the low temperature resistance behavior have been noted in other carbon-based materials. For instance, an additional component of the resistivity occurring in glassy carbon[36] has been interpreted as arising from a Mott-type variable range, hopping contribution, but the effect is in the opposite sense to the positive temperature coefficient found in the fibers. A maximum in resistivity is found in the *c*-axis resistivity of highly oriented pyrolytic graphite near 25 K[37, 38]. However, ρ_c flattens again below ~8 K, and the fiber resistivity continues to fall at 1.5 K. Therefore, it is unlikely that the effect arises from the decrease of resistance between parallel aromatic planes in the fiber. Uher[39] has also noted a similar maximum in the resistivity of pressed, exfoliated graphite very similar to that observed for the fibers, which is presumably related to the same cause.

It is known that small polarons can give rise to a resistivity maximum[40, 41]. The decrease of resistivity below the peak can be attributed to a decrease in the effective mass because the band width increases. We do not feel that this is relevant to the present case, since the electron-phonon coupling would not be sufficiently strong for the formation of small polarons. However, the idea of a resistivity maximum arising from the coupling between an electron and some other excitation is more general. Such excitations could include electron-hole (exciton) or electron-spin wave.

The latter case is of specific interest since an anomaly is observed in the specific heat below about 0.5 K in a wide variety of disordered carbons (for a review, see Mrozowski[42]). Mrozowski concluded that the peak in the specific heat occurring at ~0.2 K, whose magnitude is dependent on magnetic field, arises from spin–spin interactions. However, none of the known exchange interactions could explain the observed phenomena in a quantitative way because of the low spin density (Fig. 7). We are currently attempting to assess whether spin–spin interactions between spins on edges of ribbons could be of sufficient magnitude to explain the specific heat results.

Measurements of the magnetoresistance for this type of fiber show that it is small and positive down to 1.5 K ($\Delta\rho/\rho_0 = 10^{-4}$ at 1 T, 1.5 K). However, preliminary calculations using an Ising–Lenz model for the spin–spin interactions on the ribbon edges suggest that the magneto-resistance contribution scaled from the temperature variation of the resistance below the peak should not be measurable until much lower temperature. Future work is needed to clarify the resistance behavior of these fibers below 1.5 K and to explore the magnetic field dependence. Also, measurements on fibers heat-treated to temperatures around 1350°C are called for.

5. CONCLUSIONS

Measurements of the electrical resistivity of PAN-based carbon fibers have been carried out on a wider range of fibers, and over a wider temperature range than previous work. A surprising result is the maximum observed in the resistivity of three types of low modulus fiber.

The measured properties exhibit interesting analogies with bulk heat-treated carbons. If HTT is below ~2000°C, properties are very similar. Differences for HTT ≥2000°C are related to differences in the graphitizability among the different carbon types.

The theoretical interpretation of results on electronic properties of bulk-treated carbons is not well developed. A major advance in our understanding of negative and positive magnetoresistance has been made by Bright[28, 29] using a phenomenological model. A more fundamental description of the energy states due to Chausse and Hoarau[30] enables the overall features of Bright's model to be understood. Detailed calculations of the electronic properties (including the Hall effect and thermoelectric power) using this model need to be made. It appears that the model will have to take into account the inhomogeneity of the material, particularly the relative position of the band overlap region with respect to the vacuum level. The variation of this energy can give rise to local variations of carrier density, mobility and conductivity. Such spatial variations, together with unusual features of the energy spectrum in a magnetic field may enable the unusual properties of bulk carbons and carbon fibers to be understood.

Acknowledgements—Thanks are due to Prof. J. W. McClure for valuable discussions and for communicating results prior to publication. A grant from the Army Office of Research to Celanese Research Company is gratefully acknowledged, and also a grant from Celanese Research Company to Colorado State University.

REFERENCES

1. Spain I. L., Electronic transport properties of graphite, carbons, and related materials. *Chem. Phys. Carbon* **16**, 119 (1981).
2. Reynolds W. N., Structural and physical properties of carbon fibers. *Chem. Phys. Carbon* **11**, 1 (1973).
3. Bacon R., Carbon fibers from rayon precursors. *Chem. Phys. Carbon* **9** (1973).

4 Bright A. A. and Singer L. S. *Carbon* **17**, 59 (1978).
5 Endo M., Hishiyama Y. and Koyama T. *J. Phys.* **D15**, 353 (1982).
6 Fischbach D. B., The kinetics and mechanism of graphitization. *Chem. Phys. Carbon* **7** (1971).
7 Ezekiel H. M. *J. Appl. Phys.* **41**, 5351 (1970).
8 Diefendorf R. J. and Tokarsky E., *Polymer Engng Sci.* **15**, 150 (1975).
9 Wicks B. J., *J. Nucl. Matl.* **56**, 287 (1975).
10 Robson D., Assabghy F. Y. I. and Ingram D. J. E., *J. Phys.* **D5**, 169 (1972).
11 Robson D., Assabghy F. Y. I., Cooper E. G. and Ingram D. J. E., *J. Phys.* **D6**, 1822 (1973).
12 Mrozowski S., *Carbon* **9**, 97 (1971).
13 Mrozowski S., *Phys. Rev.* **77**, 838 (1950).
14 Delhaes P., deKepper P. and Uhlrich M., *Phil. Mag.* **29**, 1301 (1974).
15 Griffith O. K. and Gayley R. I., *Carbon* **3**, 541 (1965).
16 Coulson C. A., Schaad L. J. and Burnelle L., *Proc. 1957 Conf. Carbon*, p. 27. Pergamon Press, Oxford.
17 See for example, Spain I. L., The electronic properties of graphite. *Chem. Phys. Carbon* **8**, 1 (1981).
18 Delhaes P. and Carmona F., Physical properties of non-crystalline carbons. *Chem. Phys. Carbon* **17** (1981).
19 Cohen M. H. and Jortner J., *Phys. Rev. Lett.* **30**, 696 (1973); **30**, 699 (1973).
20 Loebner E. E., *Phys. Rev.* **102**, 46 (1956).
21 Arnold G. and Mrozowski S., *Carbon* **6**, 243 (1968).
22 Boy F. and A. Marchand, *Carbon* **5**, 227 (1967).
23 Bulawa J., Mrozowski S. and Vagh H. S., *Carbon* **10**, 207 (1972).
24 Klein C. A., *J. Appl. Phys.* **35**, 2947 (1964).
25 McClure J. W. and Ruvalds J., Private communication.
26 Wallace P. R. *Phys. Rev.* **71**, 622 (1947).
27 McClure J. W., *Phys. Rev.* **119**, 606 (1960). [See also M. noue, *J. Phys. Soc. Japan* **17**, 808 (1962).]
28 Bright A. A. *Carbon* **17**, 255 (1979).
29 Bright A. A., *Phys. Rev.* **B20**, 5142 (1980).
30 Chausse J. P. and Hoarau J. *J. Chim. Phys. (France)* **66**, 1062 (1969).
31 Hoarau J. and Volpilhac G., *Phys. Rev.* **B14**, 4045 (1976).
32 McClure J. W., Elegba S. D. and Hickman B., *Ext. Abstr. 15th Carbon Conf.*, Philadelphia, p. 10 (1981).
33 McMichael B. D., Kmetko A. E. and Mrozowski S., *J. Opt. Soc. Am.* **44**, 26 (1954).
34 Toyoda S. and Mrozowski S., *Carbon* **7**, 239 (1969).
35 Beetz C., Reported at the *Am. Phys. Soc. Meeting*, Dallas, Texas, March 1982, and to be published.
36 Saxena R. R. and Bragg R. H., *J. Non-Crystalline Solids* **28**, 45 (1978).
37 Spain I. L., Ubbelohde A. R. and Young D. A., *Phil. Trans. Roy. Soc.* **A262**, 345 (1967).
38 Morgan G. J. and Uher C., *Phil. Mag.* **44**, 427 (1981).
39 Uher C., Private communication (March 1982).
40 Holstein T., *Ann. Phys.* **8**, 325, 343 (1959).
41 Emin D., *Adv. Phys.* **22**, 57 (1973).
42 Mrozowski S., *J. Low Temp. Phys.* **35**, 231 (1979).
43 Rosenberg H. M., *Low Temperature Solid State Physics*. Oxford Univ. Press, Oxford (1963).

APPENDIX A

Heating effects in carbon fibers

Carbon fibers have diameters which are typically $D \sim 10\,\mu$m. An electric current of $10\,\mu$A corresponds to a current density of 2.6×10^{7} A m^{-2} for $D = 7\,\mu$m typical of 35 Msi fibers tested. Using a resistance per unit length of $4.5 \times 10^{5}\,\Omega$m^{-1}, the heat dissipated is $45\,\mu$W/m, corresponding to a power density through the surface of the fiber of ~ 2 W/m^2.

Consider firstly that the fiber is in a vacuum with temperature (T_0) fixed at two points distance $l = 10$ mm apart. Assuming only longitudinal heat flow (no radiation loss), and temperature-independent thermal conductivity, κ, the temperature profile along the fiber, produced by the electrical current, is parabolic, with temperature difference between the center and ends (ΔT) given by

$$\Delta T = I^2 \frac{R}{l} \frac{l^2}{2KA}$$

If $K \sim 10$ W/mK [43], $R/l = 4.5 \times 10^{5}\,\Omega$/m, $l = 10$ mm, $A = 3.85 \times 10^{-11}$ m^2, then $\Delta T \sim 6$ K for $I = 10\,\mu$A. At low temperature the thermal conductivity of the fiber is at least two orders of magnitude lower than this, so that it may be stated with confidence that other heat loss mechanisms must be considered.

Consider next the radiation loss from the region of the fiber near the middle, and neglect longitudinal heat flow. Then

$$\Delta T \sim \left[I^2 \frac{R}{l} \frac{1}{\sigma \bar{\epsilon} A} \right]^{1/4}$$

where σ is Stephan's constant (5.67×10^{-8} W m^{-2}K^{-4}), $\bar{\epsilon}$ the mean emissivity of carbon and surroundings, A the surface area (22×10^{-6} m^2 per meter-length of fiber). In the best case, $\bar{\epsilon} = 1$, $\Delta T \sim 80$ K.

Even when the fiber is immersed in a fluid maintaining constant surface temperature, a sizeable temperature difference can exist between the center and the surface. For homogeneous current flow and temperature-independent thermal conductivity

$$\Delta T = \frac{I^2 R}{4\pi K l}$$

If $K \sim 10^{-2}$ W/mK, $I = 0.1$ mA, $R/l = 5 \times 10^{5}\,\Omega$/m relevant to low modulus fiber at low temperature, then $\Delta T \sim 2.5$ K.

These calculations indicate that transport measurements cannot be carried out on fibers in a vacuum at low temperature without considerable heating, unless current well below $1\,\mu$A are used, and that care should also be exercised when the fiber is immersed in a fluid. Measurements were carried out on low modulus fiber (Celion 3000) in a vacuum. With only a current of $5\,\mu$A, the heating effect was so severe that the resistivity maximum could not be observed, even though the ceramic substrate and radiation shields were cooled to 10 K.

In order to assess heating effects with the fiber immersed directly in liquid refrigerant, experiments were carried out with electrical currents up to several mA. When the sample was immersed in LN_2, non-linear I–V characteristics were observed above about 1 mA. These effects would amount to a reduction of dV/dI of several percent by ~ 5 mA. Above this current value, the voltage reading across the fiber became noisy, and its value dropped precipitously by a few percent. Further increase of current gave values of dV/dI about a half of the value for $I \to 0$, decreasing even further at higher current values. A typical plot is shown in Fig. 12.

All of these effects are interpreted on the basis of sample heating. The precipitous effect at ~ 7 mA corresponds to the formation of a gas sheath (N_2) at the surface of the fiber, with bubbles of N_2 gas being clearly visible. Above this current, the sample temperature is probably several hundred degrees above the bath temperature. At lower current some internal heating

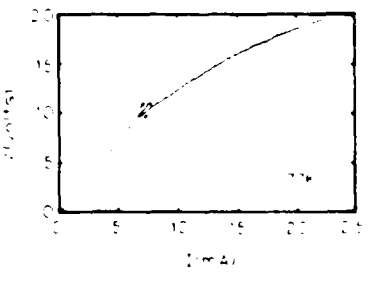

Fig. 12. Current-voltage plot for a 10-mm long carbon fiber immersed in LN.

occurs and a small temperature difference is believed to exist across the sample-refrigerant interface.

When the tests were run in LHe^4, only a small decrease of slope was observed with increasing current. Although the latent heat of LHe is much smaller than that of LN_2, the thermal conductivity is higher, enabling heat to be transported from the surface more efficiently.

These results suggest that current levels should definitely be kept below 0.1 mA and probably below 100 μA in order to avoid current heating effects with samples immersed in liquid refrigerants. Since the thermal conductivity falls to very low values at low temperature, particular care should be taken in this regime.

APPENDIX II

AN UNUSUAL RESISTIVITY MAXIMUM IN LOW MODULUS CARBON FIBERS

H. A. Goldberg and I. L. Kalnin
Celanese Research Company, Summit, NJ 07901

and Ian L. Spain and K. J. Volin
Physics Department, Colorado State University, Ft. Collins, CO 80523

Introduction

The electrical characteristics of carbon fibers have been studied by several workers (for a recent review, see Ref. 1). Electrical properties have been found to correlate well with heat-treatment temperature (HTT) [2-4]. The resistivity of fibers generally decreases with increase of HTT while the magnetoresistance is negative for a range of HTT's.

The resistance of fibers usually increases steadily as the sample temperature decreases [2,3]. However, in measurements of the electrical resistivity and magnetoresistance of fibers between 1.5 and 300 K, an unusual resistivity maximum for a low modulus fiber was discovered by us [5,6]. The fiber in question was Celion 3000, which has a Young's modulus of ∿35 Msi (240 GPa). This is a PAN-based fiber with HTT ∿1300°C (residence time ∿15 min). By this temperature, the fiber is an impure carbon with typically a few percent nitrogen and of the order of tenths of percent of various inorganic impurities. The resistance maximum has also been observed more recently in other types of ex-PAN fibers. The purpose of this note is to report on possible correlations between the unusual resistivity behavior and other physical properties.

Experimental Considerations

Electrical resistance was measured using a DC 4-point technique. Fibers were attached with conducting silver paint to four platinum strip electrodes laid down on an alumina substrate.

These measurements were taken with great care to insure reproducibility of results. It was found that small, irreproducible changes of resistivity could occur upon cycling between low temperature and room temperature. These reversible changes were random in nature, but always less than ∿1 in 10^3. Similar changes have also been observed in bulk carbon [7], indicating that they are related to the inhomogeneous nature of the carbon itself, and not due to contacts.

Precautions were taken in the measurements to insure that the fiber was not heated up. Heating effects can be extremely severe in carbon fibers in a vacuum. Currents of 10 μA, for instance, can easily raise the temperature tens of degrees. It was found that the resistivity maximum could not be observed at all if the measurements were carried out with a current of a few μA with the fiber in a vacuum. Measurements were made throughout the temperature range with the sample either immersed in gaseous helium, or below 4.2 K in liquid helium. Mechanical properties were measured using standard techniques.

Results

The types of fiber on which measurements were made are listed in Table 1, together with a synopsis of physical properties.

Table 1. Summary of Fiber Properties

Fiber	Denier D	Strain to Fracture ε	Young's Modulus E(Msi)	Fracture Stress T(ksi)	Resistivity ρ(295K) (μΩcm)	T_{MAX} (K)	$R_{MAX}/R(295K)$
Celion HTA 78023	0.56	1.18	36.7	433	1.97	30.8	1.103
Celion HTA 78023	0.77	1.06	35.6	377	1.71	35.0	1.100
Celion HE-7	0.46	1.69	42.5	720	1.67	37.4	1.097
Celion HE-7	0.62	1.62	41.2	670	1.62	35.8	1.094
Magnamite AS 4-W	0.60	1.77	39.8	708	1.83	35.6	1.117
Magnamite AS 4-W	0.67	1.82	38.4	700	1.91	34.4	1.109
Thornel	0.56	0.88	33.9	300	2.72	23.6	1.160
Thornel	0.67	0.79	33.1	260	2.33	25.9	1.156

Results on the variation with temperature of the normalized resistance R(T)/R(290 K) are given in Fig. 1. It is to be noted that the resistance reaches a maximum value for all of the fibers measured between ∿20-40 K. The location of the maximum and value of $R_{maximum}$/R(290 K) depends on the particular fiber.

Attempts were made to correlate the key features of this unusual behavior with other physical properties. Ezekiel [8] showed that mechanical properties correlated with room temperature resistivity (ρ(290 K)). Accordingly, the resistance ratios R_{max}/R(290 K) and R(4.2 K)/R(290 K) are plotted against ρ(290 K) in Fig. 2 as well as the temperature of the maximum. Although there is some scatter in the data, trends are clear.

Discussion

Resistivity behavior of the type reported is highly unusual. To the best of our knowledge it is unique to carbon.

The resistivity maximum occurs at lower temperatures for respectively lower HTT's. It is assumed that upon going to still lower HTT's the peak would disappear altogether with the resistivity vs temperature curve following that

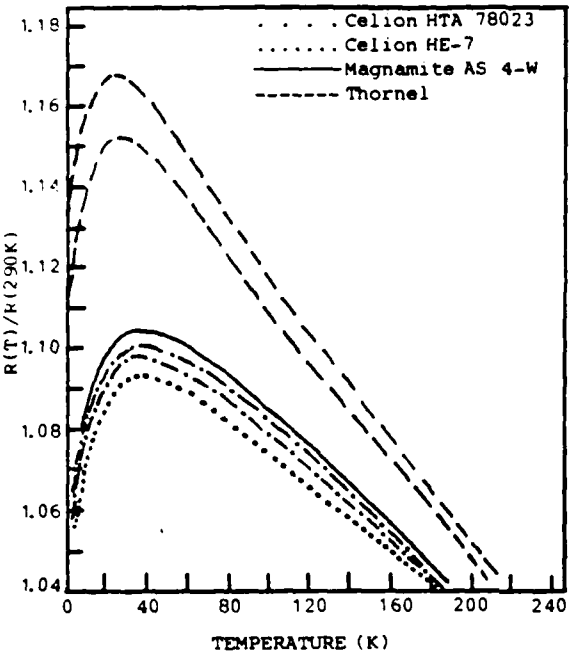

Fig. 1. The variation of reduced resistance R(T)/R(290 K) for the fibers listed in Table 1. The resistance continues to fall with increasing slope down to the lowest measurement temperature (~1.5 K).

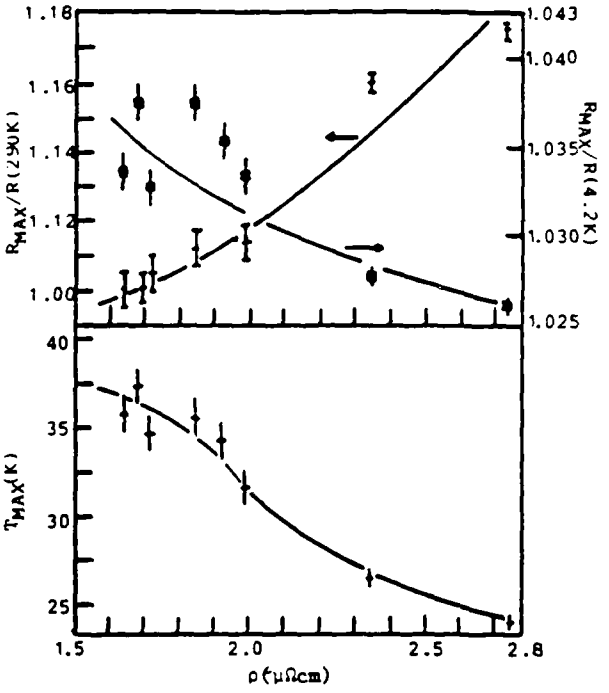

Fig. 2. Correlation of the resistance ratios $R_{max}/R(290\ K)$, $R_{max}/R(4.2\ K)$ and the temperature of the maximum, T_{max}, with room temperature resistivity.

of other disordered carbons where no maximum is observed. Upon going to higher HTT's the peak flattens out. At HTT = 2000°C no distinct peak is observed.

A resistivity maximum cannot be explained on the basis of a simple model of conduction in a crystalline material with defect scattering, nor be fitted with expressions developed for conduction in highly disordered materials. It is hypothesized that the maximum may occur if the electrons are strongly coupled to an excitation such as a spin wave. However, further work needs to be carried out to develop theoretical models quantitatively.

References

1. I. L. Spain, Chemistry and Physics of Carbon 16, 119 (1981).
2. D. Robson, F. Y. I. Assabghy, and D. J. E. Ingram, Journal of Physics D 5, 169 (1972).
3. A. A. Bright and L. S. Singer, Carbon 17, 59 (1978).
4. M. Endo, Y. Hishayama, and T. Koyama, J. Phys. D15 (Great Britain) 353 (1982).
5. H. Goldberg and I. L. Kalnin, Bull. Am. Phys. Soc. 25, 297 (1980).
6. I. L. Spain, K. J. Volin, H. A. Goldberg, and I. L. Kalnin, Solid State Comm. (in press). (A report of a resistivity maximum in Celion fiber was given by D. J. Gillespie, A. C. Ehrlich, and P. F. Waters at the Provincetown meeting on Graphite Intercalation Compounds, 1981.)
7. O. K. Griffith and R. I. Gayley, Carbon 3, 541 (1965).
8. H. M. Ezekiel, J. Appl. Phys. 41, 5351 (1970).

Acknowledgements

We thank the U.S. Army Research Office and the Celanese Research Company for financial support.

APPENDIX III

X-RAY DIFFRACTION STUDIES OF STRUCTURAL DIMENSIONALITY IN CARBON FIBERS

JAMES STAMATOFF, HARRIS GOLDBERG, AND ILMAR KALNIN
Celanese Research Company, 86 Morris Ave., Summit, N.J. 07901

ABSTRACT

Diffraction patterns of carbon fibers have been recorded photographically using monochromatized MoK_α radiation. $\langle 00\ell \rangle$ and $\langle hk0 \rangle$ reflections are observed for fibers pyrolyzed at lower temperatures. The absence of $\langle hk\ell \rangle$ reflections suggests that the graphite planes are turbostratic. A three dimensional structural transition is manifest in the appearance of $\langle hk\ell \rangle$ reflections. The results suggest that the degree of three dimensionality increases progressively through the sample as a function of increasing temperature of pyrolysis. There is no evidence for coexistence of three dimensional and the turbostratic phases. It is further demonstrated that turbostratic carbon fibers may be intercalated to stage two with AsF_5.

INTRODUCTION

Researchers exploring the intercalation of graphite normally specify the origin of graphite used, because it is well known that the microstructure and the degree of perfection of the host graphite affects not only the intercalation kinetics, but also the equilibria and the establishment of well defined stages. Even so, samples of a given type of graphite can show variability in the structural perfection which can conceivably affect the intercalation. Thus, the large spread in the electrical conductivity observed in HOPG (Highly Oriented Pyrolytic Graphite) graphite intercalated to stage 2 with AsF_5 has been attributed, at least partly, to variation in the defect density and crystallite size of the host samples [1]. Even greater variations in the properties may be caused by the structural features of the commercially available carbon graphite fiber types. Thus, the availability of such fibers offers an excellent opportunity to determine the effect of these features on the intercalation process. Both the "carbon" and "graphite" fiber structures have been investigated by x-ray diffraction and electron microscopy [2-8].

We have systematically studied fibers formed by the pyrolysis of polyacrylonitrile polymer (PAN) and pitch using x-ray diffraction methods. We examine the full range of available pyrolysis products (i.e., fibers having Young's moduli varying from 30 to 100 million psi(Msi). We also report the intercalation behavior of these fibers with AsF_5 and relate this behavior to the structure of the host fiber. The most detailed results will be given for PAN fibers. However, similar results have been obtained for pitch based fiber.

EXPERIMENTAL

For this study all x-ray diffraction measurements were performed photographically using MoK_α radiation. Carbon fibers were mounted within a glass capillary which was removed very near the incident x-ray beam. Measurements of the patterns were made using a Joyce-Loebl microdensitometer. Scans were transmitted to a computer for analysis.

RESULTS

Figure 1 shows diffraction patterns obtained from four different PAN based

carbon fibers with Young's moduli of approximately 30, 50, 70 and 100 Msi. The photographs are densely exposed in order to reveal higher order diffraction. The angular disorientation of carbon fibers is well known and is clearly demonstrated in these patterns. To review, the a and b axes of the basal planes are randomly oriented about the c axis (stacking axis of the basal planes). The c axis is perpendicular to the fiber axis but is randomly oriented about the fiber axis. Thus, <00ℓ> reflections appear as spots whereas <hk0> reflections appear as circles.

As a function of increasing modulus, the <00ℓ> reflections are observed to sharpen. This is demonstrated in figure 2 for a scan of the <002> reflection along the <00ℓ> axis. As a function of increasing modulus, the width of the <002> reflection decreases and its Bragg spacing decreases. This change with increasing modulus has been previously observed over a more limited range [9].

The degree of angular orientation also changes as a function of increasing modulus. In figure 3, the results of normalized azimuthal densitometer scans through the <002> reflection are displayed. Correlations of mosaicity with increasing modulus have been previously established over a more limited range [10].

Measurement of higher order <00ℓ> reflection widths for pyrolytic carbons suggest that line widths are broadened by liquid-like disorder (i.e., disorder of the second kind or paracrystalline disorder) in addition to contributions from finite crystallite size [11]. The same type of behavior is observed for fibers. In figure 4, the widths of the <002> and <004> reflections are plotted. The degree of liquid-like disorder and the crystallite size increases as a function of increasing modulus. Numerical results of the layer spacing, $d_{<002>}$, crystallite size along the c axis, L_c, and mosaicity of the <002> reflection, $\alpha_{<002>}$, are tabulated in the table.

The pattern shown in figure 1, also demonstrates the appearance of <hkℓ> reflections with increasing modulus. For turbostratic graphite, <hkℓ> reflections are replaced by hk lines which are parallel to the c* axis. Due to angular averaging, the hk lines form concentric cylinders coaxial with the c axis which are then angularly averaged about an axis perpendicular to the cylinders. This is clearly observed for the 50Msi PAN pattern. At higher modulus, adjacent basal planes develop correlations parallel to the plane as indicated by the appearance of <hkℓ> reflections. The most discernible <hkℓ> reflection is the <112>. In figure 5, the results of radial densitometer scans through the <112> reflection are displayed. Growth of the <112> with increasing modulus is clearly observed.

It is commonly postulated that only highly graphitic carbon (three dimensional) may be intercalated. In figure 6, a diffraction pattern of 100 Msi pitch fiber which is intercalated to stage 2 with AsF_5 is shown. In the same figure is shown 50 Msi pitch fiber with no intercalant and stage 2, AsF_5 intercalated 50 Msi pitch fiber. The patterns suggest that 50 Msi pitch based carbon fiber is turbostratic. Thus, these results suggest that three dimensionality is not required for intercalation.

DISCUSSION

The increase in three dimensional order which occurs upon heat treatment of a carbon as it approaches a truly graphitic structure has received considerable attention in the literature [12]. Carbon fibers (and other carbon forms) are in a turbostratic phase when low or moderate heat treatments are used. At heat treatments above 3000°C, one can often form graphite with an ABA stacking.

Two distinct models for this transition are:

1) Large three dimensional graphite crystallites form at some minimum heat treatment temperature, and their number and/or size grow with progressively higher heat treatment temperatures.
2) The interbasal plane correlation function gradually approaches that of graphite homogeneously throughout the sample.

Since the $d_{<00\ell>}$ spacings change continuously with heat treatment, many authors have used that change to indicate three dimensional order. Ruland has argued that a better order parameter is the mean squared fluctuation in the registry of adjacent basal planes, σ_{12} [9].

The turbostratic nature of lower modulus carbon fibers is best demonstrated by the detailed nature of the diffraction pattern in which hk lines appear as continuous scattering streaks. In figures 1, 5 and 6, <hkℓ> reflections gradually appear as a function of increasing modulus. One would expect that the amplitude of <hkℓ> reflections should be proportional to the order parameter (or the square of the order parameter, depending upon the model).

In figures 1 and 5, the relative intensity of the various <hkℓ> reflections which depend upon three dimensional order can be compared. Model 1 can be ruled out by this analysis since for 70 Msi PAN based carbon fiber, the ratio of intensities for the <114> and <112> is clearly less than 0.8, which is the value for ABA graphite. Furthermore, the results shown in figure 4 show that considerable liquid-like disorder exists indicating the absence of an ideally three dimensional graphite phase. Of course, there are numerous models which are intermediate between 1 and 2. Further work is required to put quantitative limits on the size of such regions which would remain consistent with our data.

We have demonstrated (figure 6) that turbostratic graphite fibers may be intercalated with AsF_5. For all fibers which we have intercalated, we have obtained a stage 2 compound. The degree of misorientation and crystal order varies in the intercalated fibers in qualitatively the same way as they vary in the neat (pristine) samples. There is no evidence in any samples for unintercalated turbostratic material. Thus, we can definitely rule out any model which claims that the fiber has regions of different three dimensional order and only the more ordered regions intercalate.

SUMMARY AND CONCLUSIONS

We have shown x-ray evidence for:

1) The reasonably continuous growth of three dimensional order in graphite fibers,
2) the homogeneous intercalation of completely turbostratic fibers with AsF_5 (as well as higher modulus-three dimensional ordered fibers),

suggesting the possibility of intercalating a fiber does not depend upon its degree of three dimensional order. Future work, especially the measurements of <hkℓ> peak shapes and intensities will benefit by the use of diffractometer methods.

ACKNOWLEDGEMENTS

We gratefully acknowledge F. Warner and G. Breckenridge for their superb technical assistance. We thank I. Spain and H. Noether for many valuable discussions.

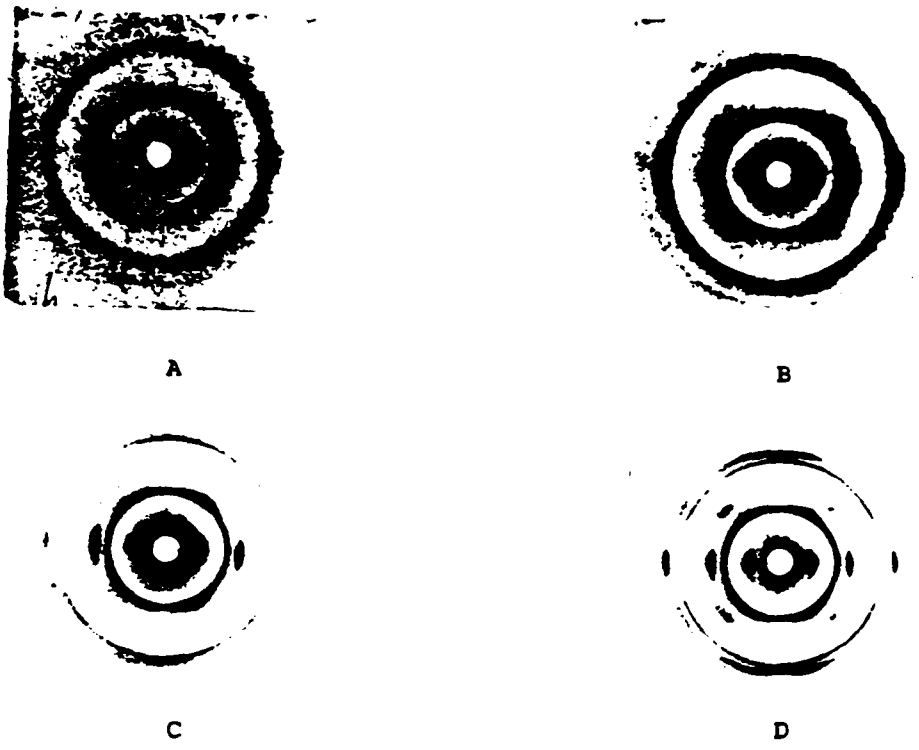

Fig. 1. X-ray diffraction patterns of PAN based carbon fibers of different modulus. Patterns were recorded with MoK_{α} radiation with the incident beam perpendicular to the fiber axis. A) 30 Msi, B) 50 Msi, C) 70 Msi, D) 100 Msi.

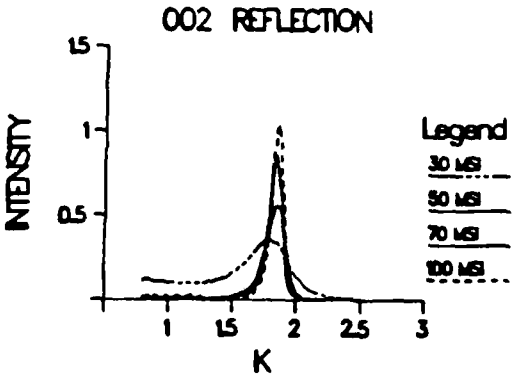

Fig. 2. The <002> reflection as a function of modulus. Integral intensities are normalized.

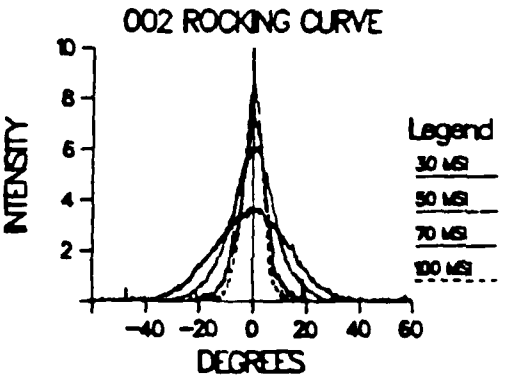

Fig. 3. Mosaicity of the <002> reflection as a function of modulus. Integral intensities are normalized.

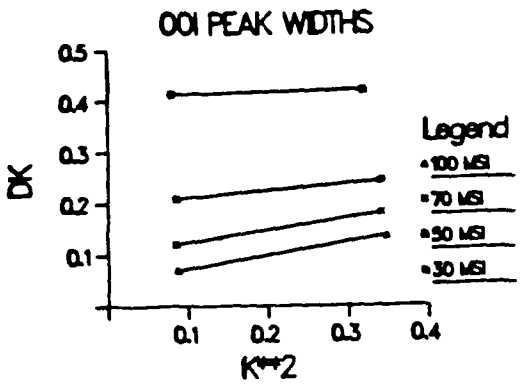

Fig. 4. Widths of <00ℓ > reflections as a function of modulus.

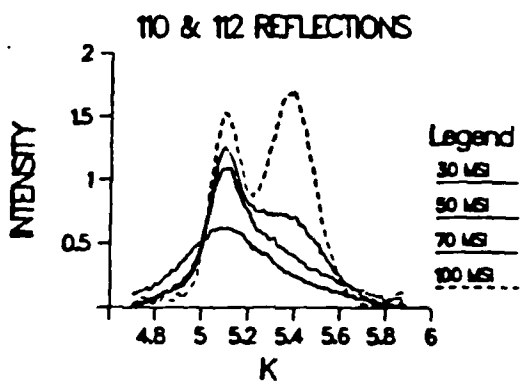

Fig. 5. The <112 > reflection as function of modulus.

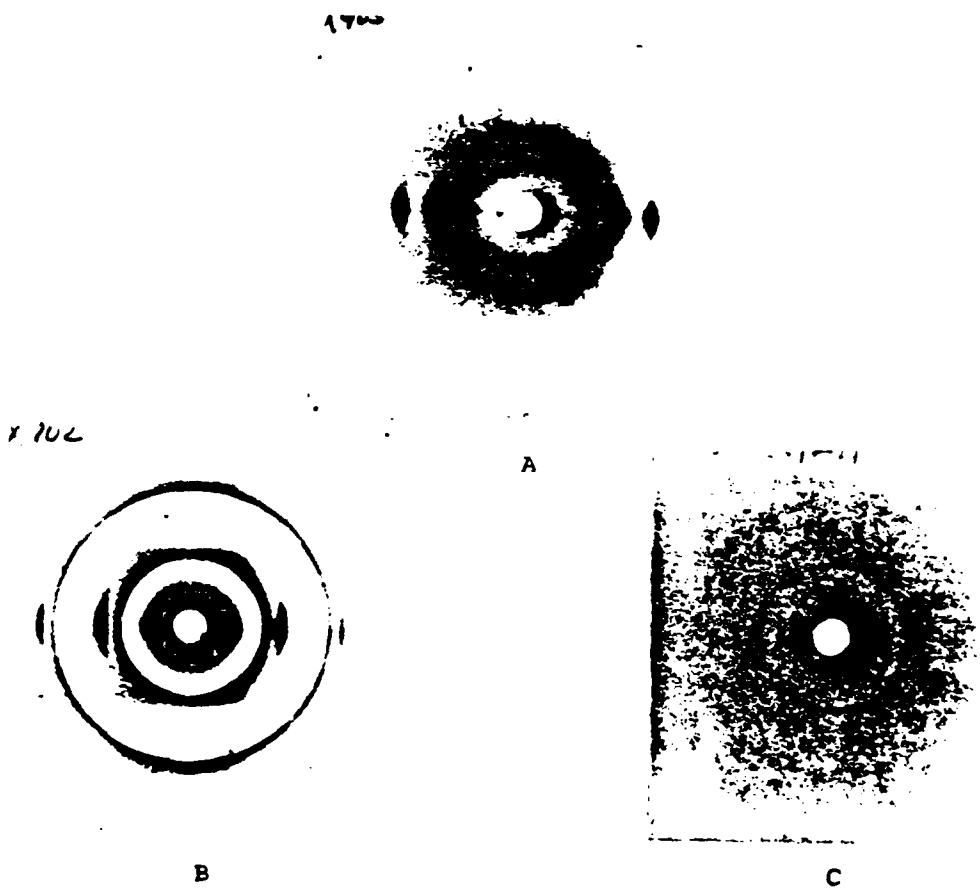

Fig. 6. X-ray diffraction patterns of pitch based carbon fibers. A) 100 Msi pitch based fiber intercalated to stage 2 with AsF_5. (Recorded with CuK_α radiation). B) 50 Msi pitch based fiber showing turbostratic order. C) 50 Msi pitch based fiber intercalated to stage 2 with AsF_5. (B and C are recorded with MoK_α radiation which excites As x-ray fluorescence degrading the signal to background ratio for C.)

TABLE I
Structural parameters of PAN based carbon fibers

MODULUS (Msi)	$D_{(002)}$ Å	L_c Å	$\alpha_{(002)}$ DEGREES
30	3.54	28	20.6
50	3.42	58	11.4
70	3.42	113	7.5
100	3.39	226	5.8

REFERENCES

1. M. J. Moran, J. W. Milliken, C. Zeller, R. A. Grayeski, J. E. Fischer, Synthetic Metals (1981) 3, 269.

2. R. Perret, W. Ruland, J. Appl. Cryst. (1970) 3, 525.

3. D. J. Johnson, C. N. Tyson, Brit. J. Appl. Phys. (1970) 3, 526.

4. A. Fourdeaux, R. Perret, W. Ruland, Proc. 1st Intern. Conf. on Carbon Fibers, London, The Plastics Institute (1971), No. 9.

5. D. J. Johnson, C. N. Tyson, J. Microsc. (1971) 94, 51.

6. S. C. Bennett, D. J. Johnson Carbon (1976) 14, 117.

7. S. C. Bennett, D. J. Johnson, ibid. (1979) 17, 25.

8. S. C. Bennett, D. J. Johnson, 5th Intern. Carbon and Graphite Conf., Vol. I, Soc. Chem. Ind., London, (1978), 377.

9. L. Fischer and W. Ruland, Colloid and Polymer Sci. (1980) 258, 917.

10. W. Ruland, Applied Polymer Symposia (1969) 9, 293.

11. W. Vogel and R. Hosemann, Carbon (1979) 17, 41.

12. J. Biscoe and B. E. Warren, J. Appl. Phys. (1942) 13, 364.

APPENDIX IV

X-ray Absorption Studies of Low Concentration AsF_5 Intercalation Compounds

S. Heald,*
Brookhaven National Lab,
Upton, N. Y.

and

H. A. Goldberg, I. L. Kalnin, and J. B. Stamatoff
Celanese Research Company**
Summit, N. J. 07901

* This research was performed in part under the auspices of of the U. S. Department of Energy, Division of Material Sciences, Office of Basic Energy Sciences under contract number DE-AC02-76CH00016

** Supported in part by the U. S. Army Research Office

ABSTRACT

Near-edge x-ray absorption data on graphite fibers intercalated with AsF_5, show that similarly to bulk graphite (HOPG), a portion of the intercalated AsF_5 disproportionates to form AsF_6^- and AsF_3. The residual amount of AsF_5 in the fiber sample is significantly smaller than that observed in the HOPG. The AsF_3 in the fiber sample is oriented with respect to the graphite planes, and the F-As-F bond angle is found to be larger than that in free AsF_3.

Interest in graphite intercalation compounds has greatly expanded since it was reported that graphite samples intercalated with AsF_5 or SbF_5 have conductivities comparable to copper[1]. Although it has since been shown that the maximum conductivity of these compounds is about one-half that of copper[2], interest remains high, particularly as to the mechanisms causing the large conductivity increases. X-ray absorption studies on AsF_5 intercalated in powdered highly oriented pyrolytic graphite (HOPG) by Bartlett and coworkers[3] indicate that intercalation is accompanied by the reaction

$$3\ AsF_5 + 2e^- \longrightarrow 2\ AsF_6^- + AsF_3.$$

Since little AsF_5 was found, it was concluded that the equilibrium of the reaction is shifted far to the right, resulting in a charge transfer of 2/3 e for each AsF_5 intercalated. All other measurements of charge transfer, however,[4-11] gave smaller values for the charge transferred, averaging $\sim$0.3 e, suggesting that substantial amounts of AsF_5 remain unreacted.

In this paper, we report x-ray absorption measurements near the As K edge on AsF_5 - HOPG and on AsF_5 - graphite fiber intercalation compounds made at the Cornell High Energy Synchrotron Source (CHESS). In addition to being the first such work on intercalated fibers, it differs from previous x-ray absorption measurements in that our samples have low concentrations of AsF_5 in order to emphasize the role of defects and/or of microstructure in determining the structure and the chemistry.

The graphite fiber was Celion® GY-70 having an average Young's modulus of ca. 600 GPa. A fiber bundle, ca. 3 cm

long, was weighed and sealed in a rectangular Pyrex ampoule with thin wall windows (~0.2 mm) to minimize the x-ray absorption and a sidearm for the introduction of the gaseous AsF_5. The ampoule was attached to a vacuum line, degassed, filled with a predetermined amount of as-received AsF_5 (from Ozark-Mahoning Co., >99% pure) by condensation with liquid nitrogen, and then sealed off and reweighed. In the particular ampoule selected for complete analysis the weight increase indicated that this sample contained 1.9% AsF_5 by weight. The x-ray absorption at the As edge indicated an AsF_5 concentration of 1.4%. Since it is not certain that all the AsF_5 intercalates, the agreement of these two numbers is reasonable. X-ray diffraction photographs of this sample were taken using monochromatic Mo K_α radiation. The c axis spacing was found to be 3.38 ± .02 Å before intercalation and 3.40 ± 0.02 Å after intercalation. The major source of uncertainty in the c axis spacing arises from the 2 mm thickness of the sample needed for the absorption measurement. No evidence for staging was observed indicating that our sample was not a mixture of pure graphite and high concentration (low stage) intercalated material. This, together with the agreement of the concentrations determined by weight uptake and x-ray absorption, indicates that the AsF_5 distribution is homogenous.

For the HOPG sample, the container and the handling were similar, except that the AsF_5 was introduced by measuring the pressure drop in a known volume during the intercalation, and sealing the ampoule off after the desired amount of AsF_5 had been taken up by the sample. The weight increase of this sample was 7.4%, while the x-ray absorption at the As edge showed a concentration of only 0.8%. This

sample was clearly inhomogeneous, hence the x-ray absorption is dominated by regions which have a higher concentration of AsF_5 than the sample average. Since both samples contained much less than one absorption length of As, any corrections to the measurements due to inhomogeneity should be small. The changes in absorption, μx, above and below the edge were 0.078 and 0.144 for the HOPG and fiber samples respectively. Measurements were also made on AsF_3, AsF_5 gas and $NaAsF_6$ as standards. The near edge absorption for these compounds is shown in Figure 1 (a). All three have strong absorption peaks at the edge. The peak for As^{+3} is well separated from the two As^{+5} peaks and, thus, easily distinguishable. Figure 1 (b) gives the results obtained on the fiber sample for the two possible orientations - the x-ray polarization vector along the fiber axis and perpendicular to the fiber axis. Two peaks are clearly seen and can be identified with AsF_3 and AsF_6^-. The AsF_3 peak also shows a clear orientation dependence. For the HOPG sample shown in Figure 1 (c), the result is somewhat different from the fiber data which are plotted for comparison. It is evident that there is an additional contribution to the low energy side of the As^{+5} peak which is presumably due to an AsF_5 signal. Also, the amount of AsF_3 is reduced.

To quantitatively analyze the HOPG and fiber results, a fit was made to the data using a linear combination of the standard edges shown in Figure 1 (a). The results are given in Table 1 and an example of a fit is shown in Figure 1 (b). The AsF_5 and AsF_6^- parameters are somewhat correlated, and the sum of their contributions is more accurately determined than their individual values. The AsF_3 values

are nearly independent of the conditions of the fit and are estimated to be accurate to about 6%. Since systematic errors associated with the normalization of the data are the same for both fiber orientations, the relative amounts of the AsF_3 values in these two cases are accurate to about 4%.

The fibers are known to have the c axis randomly oriented perpendicularly to the fiber axis. This allows us to analyze the polarization dependence in terms of the orientation of the AsF_3 molecule. In the free state the molecule has a pyramidal shape with an F-As-F bond angle of 96.2°[12]. The near edge peak is due to transitions from the original 1s state to unfilled p-states associated with the As-F bond. These p-states undoubtedly lie along the bond direction, thus giving a polarization dependence to the absorption signal of

$$\sum_i \cos^2 \theta_i$$

where θ_i is the angle between the x-ray polarization vector and the As-F bond, and the sum is over the three bonds. From our observations it is evident that plane defined by the fluorines tends to be parallel to the graphite basal planes. If the molecules are assumed to be exactly aligned in this way, the expected ratio: parallel signal/perpendicular signal is 1.17. Our observed value of 1.32 ± 0.05 is somewhat larger. This suggests that the F-As-F bond angle is larger in the intercalated state, particularly since experimental problems such as misalignment of the fibers, imperfections in the fibers, or imperfect x-ray polarization would reduce the observed ratio. If this is the case, interactions with the graphite fibers flattens the AsF_3 molecule slightly giving an F-As-F bond angle of at

least 101°.

Another possible explanation of the polarization dependence could be the presence of oriented, AsF_4^- species. Recent Mossbauer results[13] indicated that $SbCl_5$ intercalated HOPG may contain some $SbCl_4^-$. There appears to be no measurable contribution from any such species to the As^{3+} peaks observed here, although such a configuration cannot be completely ruled out at this point. However, our results seem to confirm Eq. 1. Averaging the fiber to take account of the AsF_3 orientation gives an AsF_3/AsF_6^- ratio of 0.56 ± 0.05. Since we have not yet measured the orientation dependence of our HOPG sample, we note that the AsF_3/AsF_6^- ratio is 0.44 ± .05 if we assume the same bond angle orientation as observed in our fiber sample, while the ratio is 0.47 ± .05 assuming complete orientation of AsF_3 with a 95.6° bond angle, and 0.52 ± .05 if we assume no orientation.

One of the goals of this work is to determine any dependence of intercalation compound structural and chemical properties on the nature of the starting graphite. McQuillan[15] reported seeing no orientation dependence for the As^{+3} peak in a $C_{8.7}AsF_5$ compound made from HOPG. Further work is clearly needed to determine the origin of this different behavior. Also, in contrast to previous x-ray absorption studies[3] our HOPG sample contains substantial amounts of AsF_5. It might be expected that for dilute samples as measured here the reaction of AsF_5 would be nearly complete[14]. This occurred for the fiber sample which seemed much more homogeneous than the HOPG sample. It may be that the HOPG material reacted only near the surface and is characteristic of a concentrated intercalated sample.

In conclusion, we note that further measurements on additional carefully prepared samples are required to unambiguously determine any dependence of structure and chemistry on the starting graphite, AsF_5 concentration and intercalation procedure. The data obtained so far do show the great potential of the x-ray absorption measurements for determining the relative amounts of AsF_3, AsF_5, and AsF_6^-, and, in the case of AsF_3, the orientation of the molecule as well.

ACKNOWLEDGMENT

We would like to thank George Breckenridge for his expert assistance in preparing the samples, Foster Warner for taking the x-ray diffraction photographs, and the CHESS staff for their cooperation and assistance. We are also grateful to Dr. I. L. Spain of Colorado State University for helpful discussions, to Dr. A. W. Moore of Union Carbide for providing the HOPG, and to the Celanese Research Company for permission to publish this paper. The partial financial support of the Army Research Office is gratefully acknowledged.

REFERENCES

[1]F. L. Vogel, J. Mat. Sci. 12, 982 (1977); E. R. Falardeau, G. M. T. Foley, C. Zeller, and F. L. Vogel, J. Chem. Soc. Chem. Comm., 389 (1977).

[2]T. E. Thompson, E. M. McCarron, and N. Bartlett, Synthetic Metals 3, 255 (1981) and references therein.

[3]N. Bartlett, R. N. Bianconi, B. W. McQuillan, A. S. Robertson, and A. C. Thompson, J. Chem. Soc. Chem. Comm., 200 (1978): N. Bartlett, B. W. McQuillan, and A. S. Robertson, 6th Annual SSRL Users Group Meeting, Oct. 25-26, 1979, SSRL Report No. 79/05.

[4]R. S. Markiewicz, H. R. Hart, Jr., L. V. Interrante, and J. S. Kasper, Synthetic Metals 2, 331 (1980).

[5]R. S. Markiewicz, J. S. Kasper and L. V. Interrante, Synthetic Metals 2, 363 (1980).

[6]S. Tanuma, Y. Iye, O. Takahashi and Y. Koike, Synthetic Metals 2, 341 (1980).

[7]B. R. Weinberger, J. Kaufer, A. J. Heeger, J. E. Fischer, M. Moran and N. A. W. Holzworth, Phys. Rev. Lett. 41, 1417 (1978).

[8]L. R. Hanlon, E. R. Falardeau and J. E. Fischer, Solid St. Comm. 24, 377 (1977).

[9]J. Blinowski, N. HyHar, C. Rigaux, J. R. Vieren, R. Letooles, G. Furdin, A. Herold and J. Melin, J. Phys. (Paris) 41, 47 (1980).

REFERENCES

[10]M. J. Moran, J. E. Fischer and W. R. Salaneck, J. Chem. Phys. 73, 629 (1980).

[11]C. Zeller, L. A. Pendrys and F. L. Vogel, J. of Mat. Science 14, 2241 (1979).

[12]F. B. Clippard and L. S. Bartell, Inorganic Chem. 9, 805 (1970).

[13]P. Boolchand, W. T. Bresser, D. McDaniel, K. Sisson, V. Yey, P. C. Eklund, Solid St. Comm. 40, (12) 1049, (1981).

[14]H. A. Goldberg, I. L. Kalnin and I. L. Spain, Bull. of Am. Phys. Soc., 1982 and to be published.

[15]B. W. McQuillan, Ph.D., Thesis, Univ. of Cal. at Berkeley and Lawrence Berkeley Lab report LBL-12228, 1981.

Figure Caption

X-ray absorption spectra of: a) AsF_3 (dashed line) AsF_5 (solid line) and $NaAsF_6$ (dotted-dashed line) standards; b) AsF_5 - intercalated Celion® GY-70 fibers with the x-ray polarization parallel (dashed line) and perpendicular (solid line) to the fiber axis (A fit to the data using the above standards is shown by the dots); c) AsF_5 - intercalated HOPG (solid line) and fibers (dashed line) with polarization perpendicular to the fiber axis. The data has been scaled so that the change in absorption from above to below the As edge equals one. The zero of energy is taken to be 11.868 K ev.

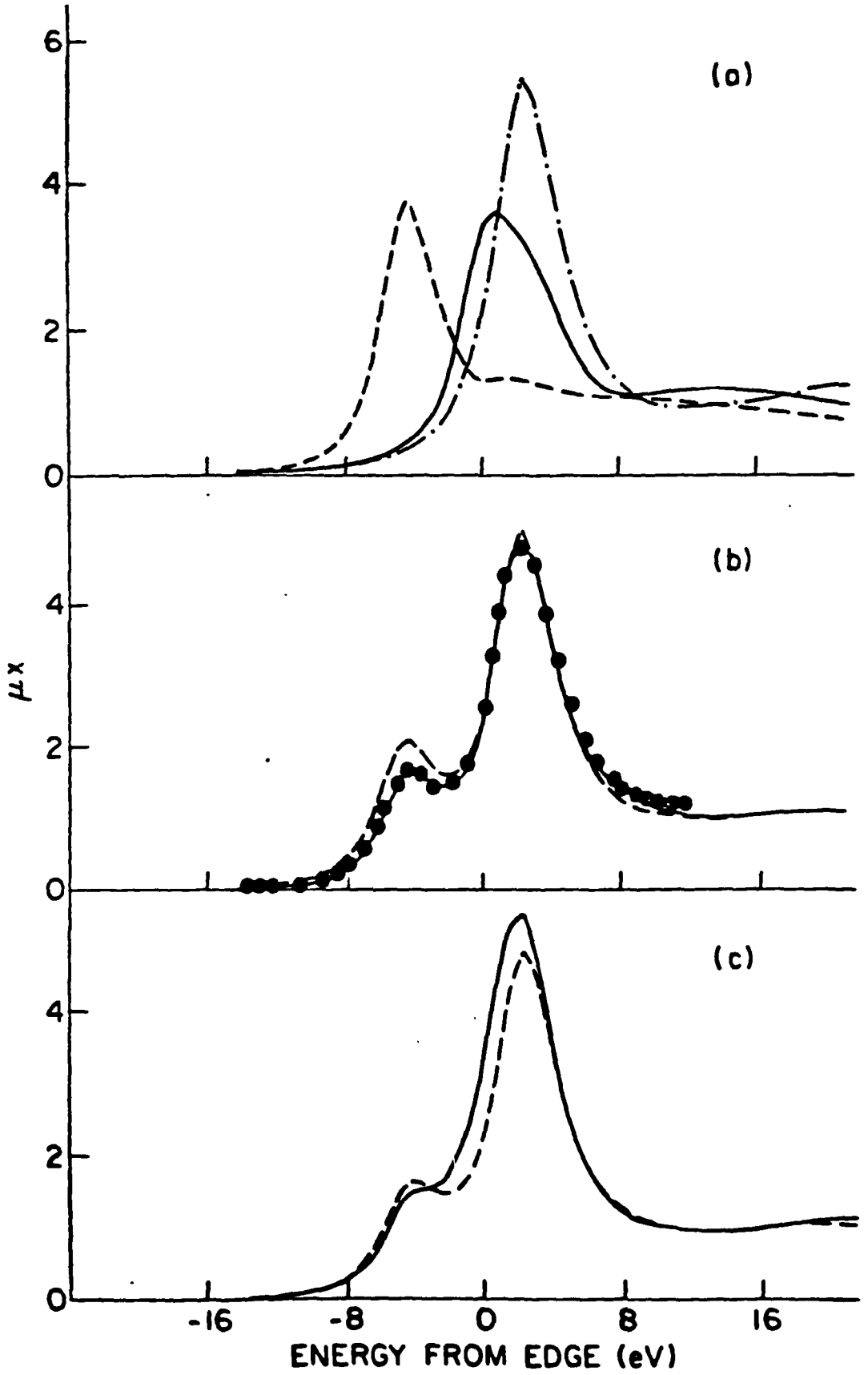
(a)
(b)
(c)
μx
6
4
2
0
-16
-8
0
8
16
ENERGY FROM EDGE (eV)

Table 1

The Relative Concentrations of Intercalated Species Obtained From X-ray Absorption Data (Figure 1)

Species:	AsF_3	AsF_5	AsF_6^-
Graphite:			
Fibers-perpendicular orientation	0.30	0.08	0.62
Fibers - parallel orientation	0.36	0.09	0.55
HOPG	0.19	0.45	0.36

The relative concentrations of AsF_3, AsF_5 and AsF_6^- obtained by fitting the data shown in figures 1b and 1c with the data obtained from measurement of standards (shown in figure 1a) are given. Note the approximate 2:1 ratio of AsF_6^- to AsF_3 in both fibers and HOPG in agreement with equation 1.

END

FILMED

8-85

DTIC